Voltage Sag Source Location in Power Systems

– Master Thesis work by Readlay Makaliki–

December, 2006

Institutionen för Energi och Miljö
International Masters Program in Electric Power Engineering
CHALMERS TEKNISKA HÖGSKOLA
Göteborg, SWEDEN, 2006
Examiner: Tuan Le Ahn

ABSTRACT

This report documents a comprehensive study of available methods for locating voltage sag sources in power systems. The performance of four sag source location methods is analyzed by simulating faults in a Brazilian transmission network using PSCAD/EMTDC.

The most reliable methods (distance relay, reactive power and slope of system trajectory) were then applied to a case study on a Zambian utility-industrial customer interface to assess the vulnerability of one of the latter's critical induction motors to voltage sags. It is shown that the sensitive load at Indeni is vulnerable to voltage sags arising from faults in both the CEC and Zesco networks, the two utilities that handle power before it gets to the customer.

Further laboratory measurements were done on the analogue network model to assess the applicability of these methods to real networks. Particularly the distance relay method which showed very good performance in PSCAD/EMTDC simulations.

Results indicate that the distance relay method is suitable for application to real networks as it showed correct sag source indications in both simulations and measurements. The performance of the reactive power and slope of system trajectory methods were above 90%.

ACKNOWLEDGEMENTS

I would like first of all to thank the Swedish Institute (SI) for the grant of Scholarship to come and study in Sweden. Secondly I would like to thank the organization I work for back home in Zambia, ZESCO Limited, for granting me a paid study leave ensuring that my family is financially taken care of whilst I was away on study leave.

Next I would like to thank my project Supervisor, Roberto Chouhy Leborgne, for all the criticism, guidance and encouragement during the project. I would also like to recognize the contribution of my project advisor, Daniel Karlsson for his advice on the project.

I would also like to recognize the important contributions of other PhD students namely Massimo Bongiorno, Finan Abdul Maguard, Ferry Vian and Cuiqing Du who I used to pester with questions.

My thanks also go to fellow Master's Students for a nice working atmosphere.

Last but not the least I would like to commend my family and children for enduring my absence of 18 months.

TABLE OF CONTENTS

1 INTRODUCTION

The American "sag" and the British "dip" are both names for a decrease in rms voltage. According to [1] voltage sag is defined as a reduction to between 0.1 and 0.9 p.u. RMS voltage at the power frequency for durations of half-cycle to one minute (Figure 1).

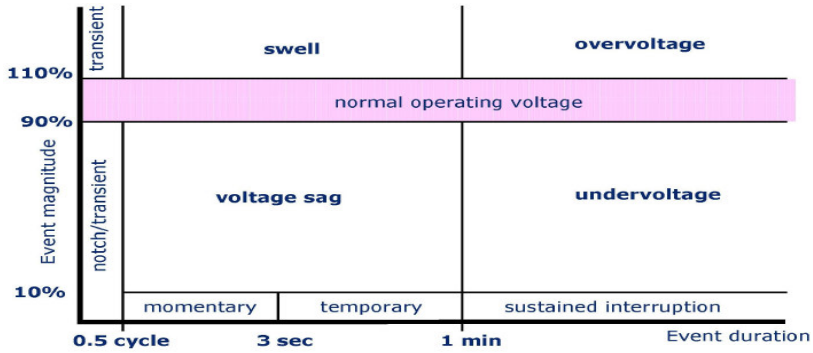

Figure 1: Event definitions according to IEEE 1159 - 1995

Voltage sags is one of the power quality problems affecting industry. Sags account for the vast majority of power problems experienced by end users. Sags are caused by short circuits, overloads, starting of large motors, capacitor switching and transformer saturation. They can be generated both internally and externally from an end users facility. Sags generated on the transmission or distribution system can travel hundreds of kilometers thereby affecting thousands of customers during a single event with catastrophic consequences. This may result in some financial compensation for parties incurring losses. Location of sag sources is crucial in developing mitigation methods and deciding responsibilities.

Though a lot of articles have been written about Voltage sag Characteristic few papers are available on voltage sag source location.

2 BACKGROUND THEORY

Voltage Sags are short duration reductions in RMS voltage mainly caused by short circuits, starting of large motors, transformer energizing and overloads. Disruptive voltage sags are mainly caused by short-circuit faults. Computers, industrial control systems and Adjustable Speed Drives (ASDs) are especially notorious for their sensitivity [2].

2.1 Characterization of Voltage Sags

Enormous efforts have been directed at the characterization and estimation of voltage sags. To this effect several papers have been written on the subjects.Voltage sag characterization studies aim at acquiring knowledge of the voltage sag characteristics. The reduction in rms voltage and the duration of the event are the main characteristics. A voltage sag is normally characterized by one magnitude and one duration. Magnitude here is defined as the remaining voltage. This characterization is fine for single phase systems and three-phase balanced faults. However for three-phase unbalanced sags the three individual phases would be affected differently leading to a case where we have three different magnitudes and three different durations. In this instance the most affected phase is taken as sag magnitude and the duration is the longest of the three durations [2]. These values can be determined by rms plots of the sampled data as shown in Figure 2.

However, several studies have shown that some other characteristics associated with sags, such as phase-angle jump, point-on-wave of initiation and recovery, waveform distortion and phase unbalance, may also cause problems for sensitive equipment [2].

The magnitude of the voltage sag is governed by the position of the observation point (pcc) in relation to the site of the short circuit and the source(s) of supply. The system can be represented by a simple equivalent circuit connecting the observation point to a single equivalent source and to the site of the fault (see Figure 3). The entire voltage (100%) is dissipated over the impedance between the source and the short circuit. The voltage drop to the observation point depends on the relative magnitudes of the two impedances connecting that point to the source and the short circuit. Depending on these impedances, the depth of the voltage sag can be anywhere in the range 0% to 100% [3].

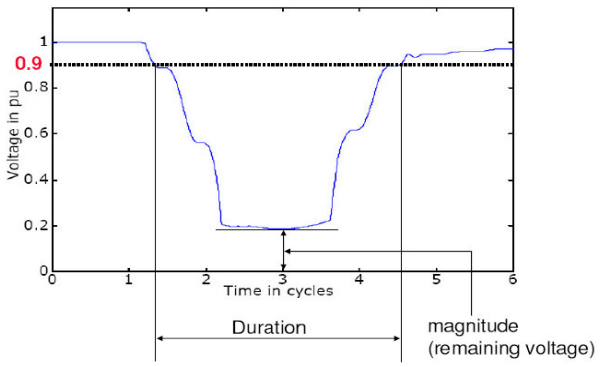

Figure 2: RMS plot of simulated waveform showing sag magnitude and duration

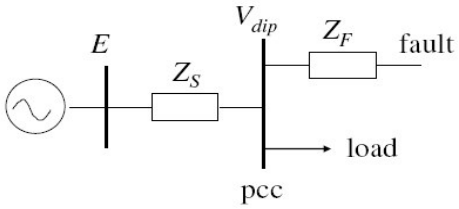

Figure 3: Simplified circuit for calculation of sag magnitude

$$V_{dip} = \frac{Z_F}{Z_S + Z_F} E \qquad (1)$$

Where Z_S = Source impedance

Z_F = Impedance between fault and observation point (pcc) and includes fault impedance

E = Equivalent Source Voltage (normally taken as 1.0 pu)

For unsymmetrical faults the voltage divider model of Figure 3 has to be split into the positive- , negative- and zero-sequence networks which combine differently according to the type of fault (LG, LL, LLG).

Unless a self-clearing fault is involved, the duration of voltage sags is governed by the speed of operation of the protective devices. In the main, the protective devices are either fuses or circuit breakers controlled by relays of various kinds.

2.2 Classification of Voltage Sags

The ABC classification as given in [2] is intuitive. It distinguishes between seven types of three-phase unbalanced voltage sags. The complex pre-fault voltage in phase a is indicated by E_1. The voltage in the faulted phase is indicated by V^* the characteristic voltage in the symmetrical component classification for all types except for type B. Table 1 shows the equations describing each sag type.

Table 1: ABC Classification of Three-phase Unbalanced voltage Sags [2]

A	$U_a = V^*$	E	$U_a = E_1$
	$U_b = -\frac{1}{2}V^* - \frac{1}{2}jV^*\sqrt{3}$		$U_b = -\frac{1}{2}V^* - \frac{1}{2}jV^*\sqrt{3}$
	$U_c = -\frac{1}{2}V^* + \frac{1}{2}jV^*\sqrt{3}$		$U_c = -\frac{1}{2}V^* + \frac{1}{2}jV^*\sqrt{3}$
B	$U_a = V^*$	F	$U_a = V^*$
	$U_b = -\frac{1}{2}E_1 - \frac{1}{2}jE_1\sqrt{3}$		$U_b = -\frac{1}{2}V^* - (\frac{1}{3}E_1 + \frac{1}{6}V^*)j\sqrt{3}$
	$U_c = -\frac{1}{2}E_1 + \frac{1}{2}jE_1\sqrt{3}$		$U_c = -\frac{1}{2}V^* + (\frac{1}{3}E_1 + \frac{1}{6}V^*)j\sqrt{3}$
C	$U_a = E_1$	G	$U_a = \frac{2}{3}E_1 + \frac{1}{3}V^*$
	$U_b = -\frac{1}{2}E_1 - \frac{1}{2}jV^*\sqrt{3}$		$U_b = -(\frac{1}{3}E_1 + \frac{1}{6}V^*) - \frac{1}{2}jV^*\sqrt{3}$
	$U_c = -\frac{1}{2}E_1 + \frac{1}{2}jV^*\sqrt{3}$		$U_c = -(\frac{1}{3}E_1 + \frac{1}{6}V^*) + \frac{1}{2}jV^*\sqrt{3}$
D	$U_a = V^*$		
	$U_b = -\frac{1}{2}V^* - \frac{1}{2}jE_1\sqrt{3}$		
	$U_c = -\frac{1}{2}V^* + \frac{1}{2}jE_1\sqrt{3}$		

With this classification the load at the same voltage level will experience different unbalanced sag type depending on whether its star or delta connected. For detailed information about voltage sag characterization and classification see [2],[4].

2.3 Propagation of Voltage Sags

There are three different types of sag propagation in power systems.

(i) Propagation at the same voltage level
(ii) Propagation to a higher voltage level (or towards the source)
(iii) Propagation to a lower voltage level (or towards the load)

For faults on distribution feeders, propagation types (ii) and (iii) are important. For transmission system faults, type (i) and type (iii) need to be considered.

Faults on the transmission network will affect a large number of customers as compared to faults in a local distribution network. Propagation in (ii) and (iii) involve passage

through transformers therefore the sag at the equipment terminals is influenced by transformer winding connections. These are classified into three types.

1) Transformers that do not change anything to the voltages. For this type of transformer the secondary side voltages (in p.u) are equal to the primary side voltages (in pu). The only type of transformer for which this holds is the star-star connected one with both star points grounded (YNyn).

2) Transformers that remove the zero sequence voltage. The voltages on the secondary side are equal to the voltages on the primary side minus the zero sequence component. Examples of this transformer are the star-star connected transformer with one or both of the star points not grounded, and the delta-delta connected transformer. The delta-zigzag (Dz) transformer also fits into this category.

3) Transformers that swap line and phase voltages. For these transformers each secondary side voltage equals the difference between two primary side voltages. Examples are the delta-star (Dy) and the star-delta (Yd) transformers as well as the star-zigzag (Yz) transformer.

The origin and transformation of the seven sag types through Dy transformers is as shown in Figure 4.

Because of transformer impedance faults propagating upwards have less effect i.e. the high voltage side will always have a higher value in p.u. terms. With propagation at the same voltage level the sag type remains the same but magnitude increases as you go towards the source in radial systems.

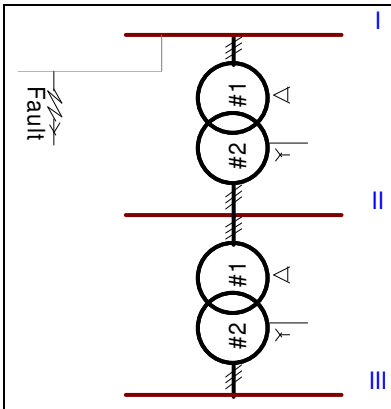

Fault Type	Location I	Location II	Location III
LLLG	A	A	A
LLG	E	F	G
LL	C	D	C
LG	B	C	D

Figure 4: Propagation of sag through Dy transformers [4]

Generally speaking the first step of power quality disturbance detection is magnitude characterization from real time field voltage and current waveforms before feature extraction.

Disturbance information from PQ monitors or any other disturbance recording device is normally available as sampled data. To be able to extract any useful information from this data therefore one requires knowledge about digital signal processing techniques.

3 SIGNAL PROCESSING TECHNIQUES

Digital signal processing (DSP), or signal processing in short, concerns the extraction of features and information from measured digital signals.

A wide variety of signal processing methods have been developed through the years both from the theoretical point of view and from the application point of view for a wide range of signals. Data are available in the form of sampled voltage or current waveforms. From these waveforms information is extracted e.g. retained voltage and duration of sag. Signal processing tools play an essential role in this step. To extract information such as type and location of the fault that caused the sag, both signal processing tools and power system knowledge are needed. Signal processing extracts and enhances the information that is hidden or not directly perceivable [4].

Depending on the stationarity of measurement data (or data blocks) one may choose frequency- (or scale) domain analysis or time-frequency- (or time scale) domain analysis. A signal is stationary when it is statistical time invariant, e.g. mean and variance of the signal do not change with time. Contrary to the stationarity, if a signal is statistical time varying, then it is non-stationary [4].

Some DSP methods currently available are briefly described below.

Many algorithms scattering in papers and standards have been proposed to characterize power disturbances. The most popular ones being RMS Values, Peak (crest) Values and Fundamental component.

3.1 RMS – Root Mean Square

The root mean square (RMS) voltage or current value is the one which is applied most broadly in power system monitoring and measurement. A great advantage of this method is its simplicity, speed of calculation and less requirement of memory, because rms can be stored periodically instead of sample per sample. However, its dependency on window length is considered a disadvantage; one cycle window length will give better results in terms of profile smoothness than a half cycle window at the cost of lower time resolution. Moreover RMS does not distinguish between fundamental frequency, harmonics or noise components, therefore the accuracy will depend on the harmonics and noise content. When using rms technique phase angle information is lost [5].

According to the definition of root mean square, the rms voltage over one data window typically one cycle is done by using the discrete integral

$$V_{rms} = \sqrt{\frac{1}{N}\sum_{n=1}^{N} v_n^2} \tag{2}$$

Real RMS is obtained if the window length N is set to one cycle. In practical application, the data window is sliding along the time sequence in specific sample interval. In order to distinguish each result, time instant stamps labeled *i* are added to RMS voltage as independent variable, i.e., it makes RMS voltage to be a function of time (instant).
The above equation then becomes;

$$V_{rms}(i) = \sqrt{\frac{1}{N}\sum_{n=i-N+1}^{i} v_n^2} \qquad \text{for} \quad i \geq N \tag{3}$$

$$V_{rms}(i) = V_{rms}(N) \qquad \text{for} \quad i \leq N \quad \text{and} \quad i \geq 1$$

The time stamp *i* is restricted to be an integer that is equal to or greater than 1. Each value from equation (3) is obtained over the processing window. It is obvious that the first *N-1* RMS voltage values have been made equal to the value for sample N. It is due to data window limitation and data truncation and couldn't be avoided. In equation (3) the time instant matching is determined by the integral discretizing process. The above equation makes the result to the last sample point of the window. The determination of initialization time and recovery time of the disturbances will be affected by time matching, while the duration will not.

3.2 FFT - Fast Fourier Transform

Fourier analysis is used to convert time domain waveforms into their frequency components and vice versa. When the waveform is periodical, the Fourier series can be used to calculate the magnitudes and phases of the fundamental and its harmonic components.

More generally the Fourier Transform and its inverse are used to map any function in the interval $-\infty$ to $+\infty$ in either the time or frequency domain into a continuous function in the inverse domain. The Fourier series therefore represents the special case of the Fourier Transform applied to a periodic signal.

In practice data are always available in the form of a sampled time function, represented by a time series of amplitudes, separated by fixed time intervals of limited duration. When dealing with such data a modification of the Fourier transform, the DFT (discrete Fourier transform) is used. The implementation of the DFT by means of FFT algorithm, forms the basis of the most modern spectral and harmonic analysis systems.

DFT transforms a signal from the time domain to the frequency domain. This makes available the amplitude and phase of the fundamental and the harmonics present in the signal. The dc component is also available in the first bin.

The Fast Fourier Transform (FFT) is the DFT's computational efficient implementation, its fast computation is considered as an advantage. With this tool it is possible to have an estimation of the fundamental amplitude and its harmonics with reasonable approximation. FFT performs well for estimation of periodic signals in stationary state; however it does not perform well for detection of sudden or fast changes in waveform e.g. transients or voltage sags. In some cases, results of estimation can be improved with windowing, i.e. Hanning, Hamming or Kaiser window [5].

Window length dependency resolution is a disadvantage e.g. the longer the data window (N) the better the frequency resolution.

Sets of sliding window DFTs can however be can be used to analyze non-stationary signals.

3.3 STFT – Short Time Fourier Transform

The Short Time Fourier Transform (STFT) is commonly known as the sliding window version of FFT, which has shown better results in terms of frequency selectivity compared with wavelets which has center frequencies and bandwidths fixed. However STFT has fixed frequency resolution for all frequencies, and has shown to be more suitable for harmonic analysis of voltage disturbances than binary tree filters when applied to voltage sags [5].

3.4 Wavelets

Since 1994, the use of wavelets has been applied to non-stationary harmonics distortion in power system. This technique is used to decompose the signal in different frequency bands and study its characteristics separately. Wavelets perform better with non-periodic signals that contain short impulse components as is typical in power system transients. Many different type of wavelets have been applied to identify power system events such as: Daubechies, Dyadic, Coiflets, Morlet and Symlets wavelets. However, wavelet type is chosen according to the specific event to study, making this technique wavelet-dependent and less general [5].

3.5 Kalman Filters

Filters seem to be suitable to extract signals in a specified band width e.g. low-pass, band-pass and high-pass filters. A well known technique is the so-called Kalman Filter. Although normally listed separately as a different method Kalman filtering is a type of least square estimator of the dynamic system parameters. The Kalman approach is recursive and thus allows each new sample to be efficiently incorporated into the estimation. This technique is designed as a state space model, and can be used to track amplitude and phase angle of fundamental frequency and its harmonics in real time under noisy environment [4].

Wavelets, STFT and Kalman filters are not used in this thesis.

4 REVIEW OF SAG SOURCE LOCATION METHODS

Previous work done on sag source location is briefly discussed below.

4.1 Distance Relay Method [6]

The paper shows that it is possible to detect the source of voltage sags using the seen impedance and its angle before and during the sag. The PQ Monitor at the affected bus can indicate the direction of the sag source. The corresponding estimates required by the PQ Monitor to compute the impedance and the angle may be obtained from the local distance relay or employing its algorithm.

With this approach, the position of the sag source in an integrated network can be obtained from simultaneous readings of different PQ monitors.

Most of the transmission systems are equipped with distance relays for protection. The relay estimates voltage and current phasors using signal processing algorithms (Kalman filters as stated in the paper) and computes the seen impedance there from to derive the trip decision. The seen impedance depends on system configuration (radial, interconnected, with distributed generation etc).

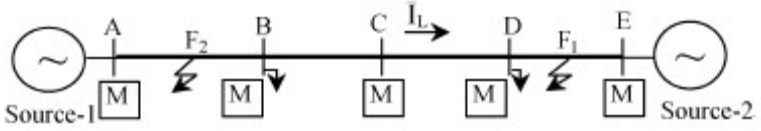

Figure 5: One line diagram of an interconnected power system

In Figure 5 consider the PQ monitor at location C. The active power flow is as indicated by the arrow below load current I_L. For a single phase fault at F_1 in phase a:

$$Z_{seen} = \frac{V_a}{I_a} = Z_{if} + \Delta Z \qquad (4)$$

Where ΔZ = function of fault resistance, load angle etc
Z_{if} = positive sequence impedance up to the fault point

The above relation (4) refers to the forward direction but in the case of a fault behind the relay, the current direction will be reversed and the resultant seen impedance will change in both magnitude and angle. Therefore, the magnitude and angle of the impedance computed from voltage and current phasors possesses a distinctive feature in identifying the disturbance direction. The rule for the sag source detection becomes:

If $|Z_{sag}| < |Z_{presag}|$ and $\angle Z_{sag} > 0$, then sag source is in front of the PQ monitor, else sag source is behind the monitor.

The paper however outlines some limitations of distance/directional relays in finding the source of the voltage sag:

(i) In radial systems and for faults behind the distance relay, there will be no change in seen impedance. As such no directional relay is also available for such a system.

(ii) A transmission line functioning as an integrated system may sometimes operate as a radial system fed from either end and in such an event the information from the directional relay may be wrong for the purpose. This is because at radial system situations a fault between relay and source does not produce any change for the directional relay.

(iii) When a fault is not permanent the local distance relay may not derive a decision.

4.2 A Novel Methodology to locate originating points of voltage sags in Electric Power Systems [7]

The paper argues that it is a common mistake to consider that the voltage sag location can be determined simply by comparing voltage and current magnitudes recorded on one single location. It could be stated that if both voltage and current magnitudes decrease, the voltage sag would be located upstream of the measurement point, and if the voltage decreases whereas the current increases the origin of perturbation should be located downstream. That would be the case if the loads connected are passive or if during the perturbation loads are represented simply as constant impedances; the real world situation is completely different. The presence of transformers, induction motors, capacitors, faults (normally cannot be represented as constant impedance), etc., greatly modifies voltage sag characteristics. The combined system reactions create changes in voltage and current that masks the origin location.

The paper states that many researchers have been working on methodologies able to identify the type of perturbation using techniques such as artificial intelligence, neural networks, wavelet, etc. However, the problem of locating perturbation origin remains uncertain. It quotes a source expressing the index of accuracy as approximately 60 to 87.5 %, in spite of using as decisive information the result of the application of several rules. Today, assignment of liability is a crucial factor due to the economic losses involved in any voltage-sag event.

The paper states that the detection procedure is based on the traditional parameters plus the analysis of voltage and current phase jumps.

4.3 Slope of System Trajectory Method [8]

The method is based on the conclusion that the relationship between the product of the voltage magnitude and power factor against current at the measurement location are not the same for different fault locations. The method first plots these two parameters during the system disturbance and then checks the slope of the line fitting the measured points. A least-squares method is used to perform the line fitting. The sign of the slope indicates the direction of the voltage sag source.

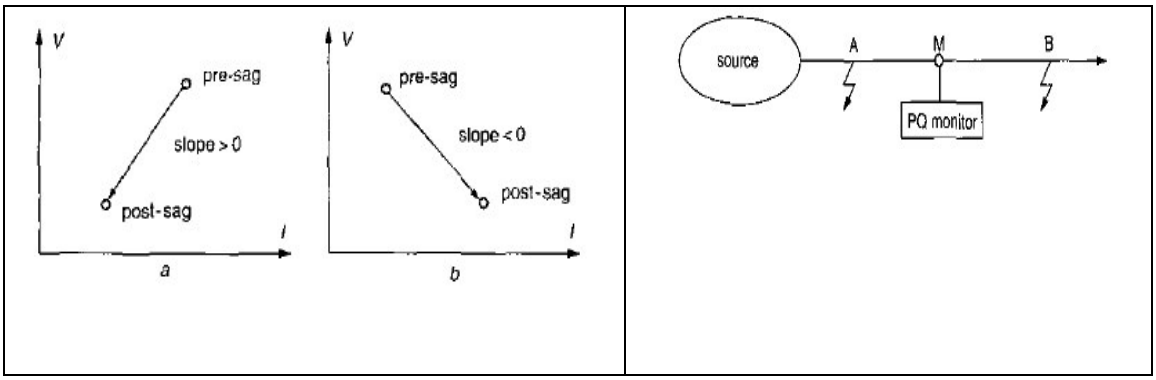

Figure 6: (a) fault at point A (Upstream fault), (b) fault at point B (Downstream fault)

Summary of Implementation steps

1. Abstract the fundamental components from the recording voltage and current once the sag is captured. Calculate angle between measured voltage and current θ for each point.

2. Plot the coordinates of (I, |Vcosθ|) during the sag.

3. Apply the Least-Squares method to fit the points with a straight line.

4. Check the sign of the slope. If its negative the disturbance is located downstream, while a positive slope represents an upstream disturbance.

5. If the active power direction reversal is detected during the event the voltage sag-source is upstream.

4.4 Resistance Sign-Based Method [9]

In this paper the principle is to estimate the equivalent impedance of the non disturbance side by utilizing the voltage and current changes caused by the disturbance. (The fundamental-frequency positive sequence impedance of the portion of the system where

the sag does not reside is calculated). The sign of the real part of the estimated impedance can reveal if the disturbance is from upstream or downstream.

The paper argues that the probability that a disturbance can occur on both sides of the measuring point simultaneously is practically zero, therefore the assumption that parameters on the non disturbance side are constant is justifiable.

The assumption of a linear system makes the proposed method less reliable. The presence of non linear loads such as variable frequency drives and induction motors can affect the sag source location as their response during voltage sag is quite different from linear loads.

4.5 Disturbance Power and Energy Method [10]

In this paper using sampled voltage and current waveforms from a monitoring device it is possible to determine whether a disturbance is in front or behind a monitoring device (i.e in the direction of positive power flow or negative power flow). This is demonstrated by examining the energy flow and peak instantaneous power for both capacitor energizing and voltage sag disturbances.

Since nonlinear loads can be thought of as sources of power at harmonic frequencies, they can be located by noting that harmonic active power tends to flow away from such a load. On the other hand, when a transient disturbance event is present in a system, it can often be thought of as an energy sink. Likewise, during a fault, energy is diverted from other loads to the fault path. Therefore, the direction of energy flow through the network during a disturbance is a key indicator of the location of the disturbance source.

The difference in the total three-phase instantaneous power and the steady-state three-phase instantaneous power is defined as the “disturbance power” (DP). Since the steady-state instantaneous power is fairly constant, the DP is approximately zero except when the disturbance is on. Therefore, a nonzero value for DP indicates the change in the instantaneous power flow caused by the disturbance event. The integral of the DP, the “disturbance energy” (DE), likewise represents the change in energy flow through the recording device due to the disturbance, since the DP makes little contribution to this integral when no disturbance is present, being approximately zero. Information about changes in the DP and DE allow us to make a decision about the location of the disturbance, as energy tends to flow toward the disturbance source.

The polarity of the initial peak of the disturbance power and the polarity of the final disturbance energy value (especially if final value is above 80% of peak excursion DE) indicate the direction of the disturbance source. If the polarity of the initial peak for DP and DE agree then the degree of confidence is high. The disturbance energy test may sometimes be inconclusive however, direction may still be determined based on disturbance power.

The criteria for indicating sag source is thus as follows:

- Negative initial peak indicates sag source behind PQ monitor.
- Positive initial peak indicates sag source in front of PQ monitor.

4.6 Event Cause Method [11]

In this article sag source location rules are derived according to the characteristics of the event cause. Three voltage sag causes are cited; line fault, induction motor starting and transformer saturation.

The paper ideally deals with radialy operated system. The UP and DOWN areas in relation to the monitor position are closely linked to the direction of energy flow. The sequence is that first the cause of the disturbance is identified and then the criteria indicating event source is applied. These criteria are as follows:

(a) Line Fault

Identified by a sharp drop and a sharp rise in the rms voltage waveform and direction indication criteria is

$$\text{Down if} \qquad \frac{I_{sag}^{1}}{I_{ss}^{1}} \geq Thr_{LF} \tag{5}$$

$$\text{Up if} \qquad \frac{I_{sag}^{1}}{I_{ss}^{1}} < Thr_{LF} \tag{6}$$

where, I_{ss}^{1} : fundamental frequency component of the current before line fault

I_{sag}^{1} : fundamental frequency component of the current during line fault

Thr_{LF} : threshold of the ratio $\frac{I_{sag}^{1}}{I_{ss}^{1}}$

(b) Induction Motor Starting

This is identified by a sharp and balanced drop in voltage with a slow exponential recovery. Sag source direction is then indicated as

$$\text{Down if} \qquad \frac{P_{post} - P_{pre}}{P_{pre}} \geq Thr_{im} \tag{7}$$

$$\text{Up if} \qquad \frac{P_{post} - P_{pre}}{P_{pre}} < Thr_{im} \tag{8}$$

Where

P_{pre} : Steady state active power before induction motor starting

P_{post} : Steady state active power after induction motor starting

Thr_{im} : threshold of the ratio $\frac{P_{post} - P_{pre}}{P_{pre}}$

(c) Transformer Saturation

This is identified by sharp and unbalanced voltage drop with a slow exponential recovery and dominance of second order harmonic in current waveforms. The sag source direction is then;

$$\text{Down if} \quad \frac{I_{sag}^{1}}{I_{ss}^{1}} \geq Thr_{tr} \tag{9}$$

$$\text{UP if} \quad \frac{I_{sag}^{1}}{I_{ss}^{1}} < Thr_{tr} \tag{10}$$

where, I_{ss}^{1} : fundamental frequency component of the current before transformer saturation.

I_{sag}^{1} : fundamental frequency component of the current during sag caused by the transformer saturation.

Thr_{TR} : threshold of the ratio $\frac{I_{sag}^{1}}{I_{ss}^{1}}$ in transformer saturation event.

4.7 Real Current Component Method [12]

This approach uses polarity of the real current component to determine the sag location relative to the monitoring point. The product of the RMS current and the power factor angle (Icosθ) at the monitoring point plotted against time is employed for the sag source location.

The product polarity is used to indicate the direction of the sag source either upstream or downstream relative to the measuring point. A positive polarity at the beginning of the sag duration indicates that the sag source is from downstream while a negative polarity indicates a sag source from upstream.

The implementation procedure is as follows:

(i) Obtain the magnitude and phase of voltage and current from the measuring device at pre-fault and during fault times.

(ii) Calculate the values of Icosθ for a few cycles of the pre-fault and during fault durations.

(iii) Graphically plot coordinates of Icosθ against time of a few cycles of pre-fault and during fault durations.

(iv) Check the polarity of Icosθ at the beginning of the fault. If it is positive the source of the voltage sag is from downstream. Otherwise if it is negative the source of the voltage sag is from upstream.

4.8 Tapping Protective Relays for Power Quality (PQ) Information [13]

The rationale for this is that relays are installed almost at every bus in the power system. As microprocessor technology continues to expand, microprocessor-based protective relays will enjoy enhanced functionality. Currently load profiling, fault oscillographic waveform capture, and metering are some of the enhanced functionality available in microprocessor-based protective relays. The article shows how existing signal processing capabilities of protective relays can be used to intelligently monitor power quality.

PQ events that industrial account managers are interested in (voltage sags, swells, interruptions) and additional events PQ engineers need (waveform capture, harmonics) can be gathered by protective relays.

PQ monitors trigger oscillographic waveform capture at a high sampling rate based on a voltage or current deviation and store the data to a hard drive or other high capacity memory. While all major events are captured, this often results in excessive data from non-critical events. The engineer must then sort through this data to analyze the power quality disturbance. For a protective relay, the typical minimum sampling rate is from 8 samples per cycle. Also, on-board memory is more limited. These constraints result in two major issues:

- Protective relays must filter PQ events to optimize event storage

- Protective relays cannot capture high-frequency events.

The first point results in the necessity of the protective relay to intelligently categorize events. This is done using the IEEE definitions as a framework. The second point results in the inability to capture lightning surges and high harmonics. However, the vast majority of PQ functions, and those most critical to industrial account mangers, do not require high-frequency data.
PQ monitoring in a protective relay is not meant to compete with high-end power-quality devices. Rather, power quality monitoring in a protective relay allows for much more

economical monitoring of multiple points within the utility. Further, once an issue is detected, powerful portable PQ devices can be deployed for analysis. Major benefits include:

- Economical monitoring of multiple points using available assets.
- Relay is attached to the power system all the time: additional information for incremental additional investment.
- Relay is connected to substation batteries: monitors events during system disturbances; does not require a separate UPS battery.
- Relay is usually attached to a communications network and information access system: utilize existing networking and communication investment more fully: minimize redundant systems and maintenance.
- Microprocessor technology continues to grow: higher speeds/lower costs will allow continued function integration into relay systems. Combined PQ event analysis and relay operation analysis: symbiotic relationships between the two.

Thus, PQ monitoring in a relay can be another tool in the utilities' arsenal for customer monitoring and response.

4.9 Analysis of the Various Methods

The distance relay method works well for two source system with one line in between and can thus be viewed as basically radial. It is however, not certain whether the method would hold for meshed networks as the case is in transmission and sub-transmission networks. It would also be interesting to see how the method performs under non linear load conditions as well as in the presence of distributed generation.

Though the distance relay may not derive a trip decision for upstream faults in a radial system if a drop in voltage can trigger recording of voltage and current waveforms during the disturbance then this information can be processed to indicate the direction of the voltage sag source. As distance relays are widely used on the power system it would make it easy to locate sources of voltage sags as little additional equipment would need to be installed.

The method in [7] relies on analyzing voltage and current waveforms in time-domain to obtain phase jumps. It is stated that for deep voltage sags, phase-jump would be a good index for finding voltage sag locations. However, this statement implies that sources of shallow voltage sags may never be located. The level of sag depth is also not quantitatively stated (how deep is deep).

Overall the paper is not very explicit. It says "the detection procedure is based on traditional parameters", when it is not clear what these traditional parameters are. Additionally, it does not say how the obtained phase-jump is used to indicate sag source direction neither does it say whether the method works well for both radial and meshed systems.

The method of slope of system trajectory plots (I, |Vcosθ|). It is interesting to investigate whether slope of the line fitting of this plot can indicate something about sag severity. It is also apparent that there is a requirement to know the direction of pre-fault active power flow.

The resistance sign based and the slope of system trajectory methods are proposed by the same authors. They state that the latter is a variation of the former which is a more general method.

The paper on the resistance sign based method also concentrates its investigation on customer- utility interface point (i.e basically radial) and does not assure whether method can apply to meshed networks.

In the resistance sign based method, choosing the number of pre- and during-sag cycles for impedance estimation is crucial. There is also a risk of failure to correctly locate sag sources with lower during-fault energy levels. Further the method may be unreliable for meshed systems.

In the event cause method the decision criteria to determine the sag source is not very convincing. It's a matter of chance to get a correct threshold setting (especially for line faults and induction motor starting).

Depending on the threshold (Thr_{LF}) selected the value of $\frac{I_{sag}^{1}}{I_{ss}^{1}}$ would be low for heavy load case and high for light load case despite the fault magnitude and position being the same leading to erroneous decision.

The real current component and the slope of system trajectory methods present results on per phase basis. Though in the papers for the two methods it is not explicitly stated which phase to use, for analysis in this thesis the faulted phase(s) will be used to indicate sag source direction.

Further in the real current component method the direction of sag source is indicated by the polarity of the initial deflection. However in this thesis the FFT algorithm is used to process the voltage and current signal to obtain angle information. The performance of the FFT in the transitory stages is not reliable and thus instead of using the polarity of the initial deflection the polarity of the during-fault steady state deflection is used.

Ideally if the sampling speed in a protective relay is enhanced to levels similar to dedicated PQ monitors then the former can be used for sag source location reducing the

source of a disturbance to a zone. Disturbance data on the relay can also be accessed from remote through SCADA.

However, very high sampling rates would compromise the protection functionality of the relay. Additionally the requirement for huge memory capacity would make the relay somewhat expensive. To get rough indications of where the trouble areas in a network are the relay is an attractive device for reasons stated in section 4.8. Detailed investigations can then follow with high-end power quality devices installed at the affected buses.

In [14] an attempt is made to compare the methods highlighted in section 4.1 to 4.7 of this report. The analysis concentrates on customer-utility interfaces which are essentially radial. The intention is not to have the exact fault location as in protection systems but to have a relative location for a given monitor. It notes that asymmetrical faults are more difficult to locate because each phase shows a particular behavior. It concludes that the available methods are not totally reliable and more research is needed to extend the methods to meshed networks.

This thesis furthers the work attempted in [14]. Four location methods will be assessed in two different networks. Laboratory measurements are conducted to further compliment PSCAD/EMTDC simulations. As an alternative to the disturbance power and energy method the reactive power method is proposed as the variation of reactive power is strongly related to the change in voltage. The Reactive Power variation method works as follows:

1. For a monitoring point operating with negative reactive power a fault is considered downstream if there is a reverse of reactive power sign (negative to positive) during the disturbance otherwise the fault is upstream.
2. If a monitoring point is operating with positive reactive power a downstream fault is indicated by a positive deflection while an upstream fault is indicated by a negative deflection of reactive power during the disturbance. No need for change of sign in this case.

5 SIMULATIONS

Simulations were twofold. Initially two network models were simulated in PSCAD/EMTDC. These are part of the Brazilian network (Mato Grosso) and the Zambian Copperbelt grid.

Simulations on the Brazilian grid were used to assess the performance of the location methods. The most promising methods were then applied on a case study on a Zambian grid to determine areas of vulnerability for sensitive loads at a petroleum process factory. The following location methods were assessed

I. Distance Relay Method (DR)
II. Slope of System Trajectory Method (SST)
III. Real Current Component Method (RCC)
IV. Reactive Power Method (RP)

5.1 Simulations in the Brazilian Network

Simulations in PSCAD/EMTDC have been done on the Brazilian Network shown in Figure 7. The network contains 67 transmission lines (138 and 230 kV) with a total length of 6619 km. There are 93 substations with a transformer-installed capacity of 2076 MVA. The generation capacity is larger than the present demand. The excess of generated power is exported to another regional grid through the substation where the bus 205 is located. The features of this network are:

- All transformers in the system are star-star connected and grounded on both sides. This means that when voltage sags are propagated in the network the sag type is maintained at all voltage levels (monitoring positions). A simplification necessary for understanding the SST and RCC methods.
- The network is highly interconnected. This is necessary for testing location methods in meshed networks.
- There is an appreciable amount of distributed generation (DG) which masks the source of voltage sags as the DG tries to keep up voltages at nearby buses during voltage sags.
- Linear load representation.
- There are two sections of the network which are essentially radial. From bus 2100 to bus 1783 and from bus 2230 to bus 840. These sections will be used to test the performance of the location methods.

Eleven fault types were simulated at each of the following selected buses, 205, 1922, 2230, and 2015. Monitors are positioned at various 230kV and 138kV buses in the network but our focus is the monitors at bus 2103 and bus 2008. Faults at the above selected buses would represent either upstream or downstream faults for our two monitoring position. The eleven fault types are:

- LG (x3) Phase A, B, C
- LL (x3) Phases AB, BC, CA
- LLG (x3), Phases AB, BC, CA
- LLL
- LLLG

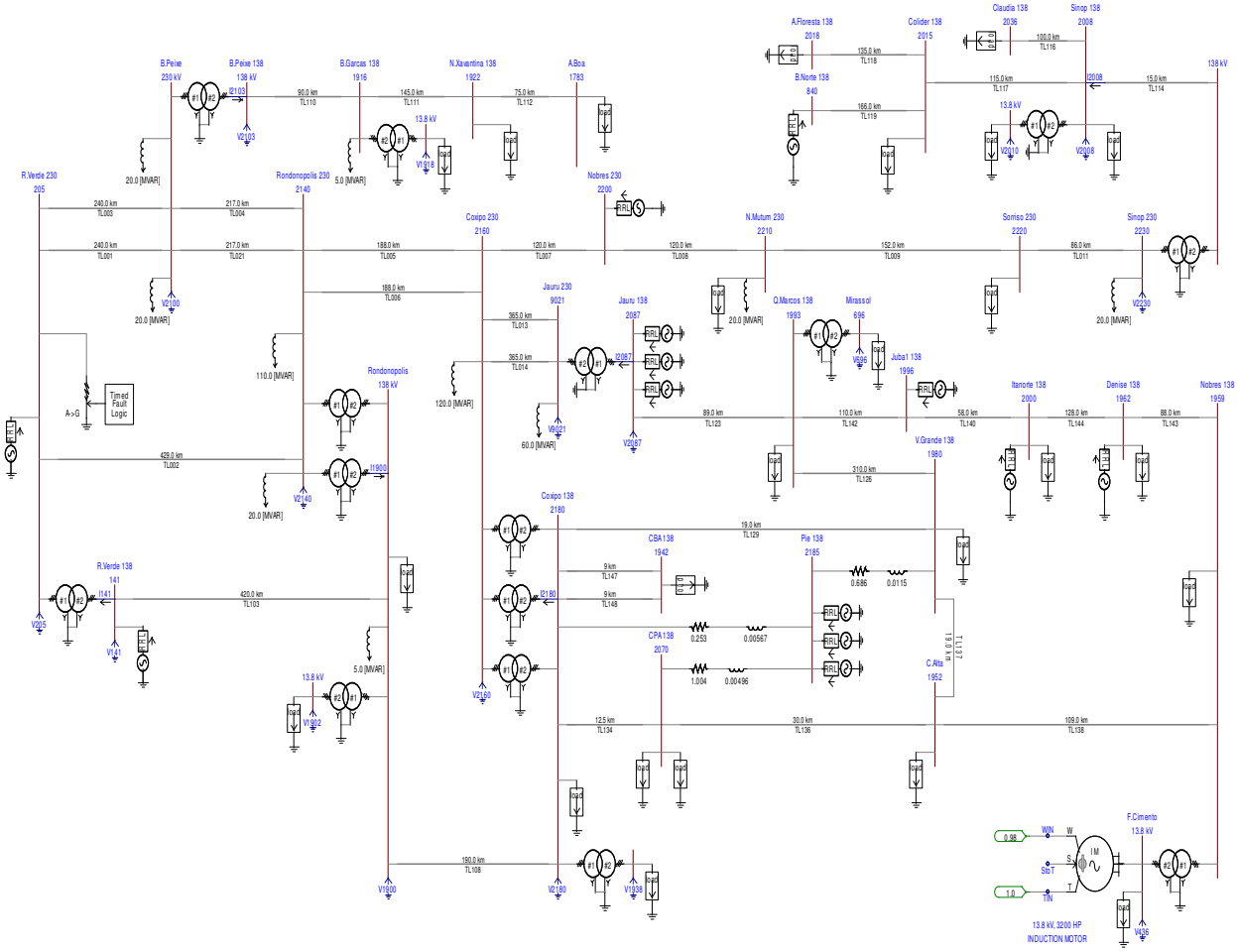

Figure 7: Brazilian Network (Mato Grosso)

The outputs of the PSCAD/EMTDC simulations were processed in MATLAB. The following are the results of the MATLAB post processing. The fault type is indicated on the top left subplot of each figure in brackets.

5.1.1 Distance relay method applied to the Brazilian network

Figure 8 shows a plot of the positive sequence impedance and its angle against time at various 138kV buses for fault type LLLG205. This is interpreted as a three-phase-to-ground fault at bus 205. This graph is representative of the distance relay method (DR). In this method the condition stated in section 4.1 for a downstream fault is $|Z_{sag}| < |Z_{presag}|$ **and** $\angle Z_{sag} > 0$. The rest of the combinations will signify upstream faults.

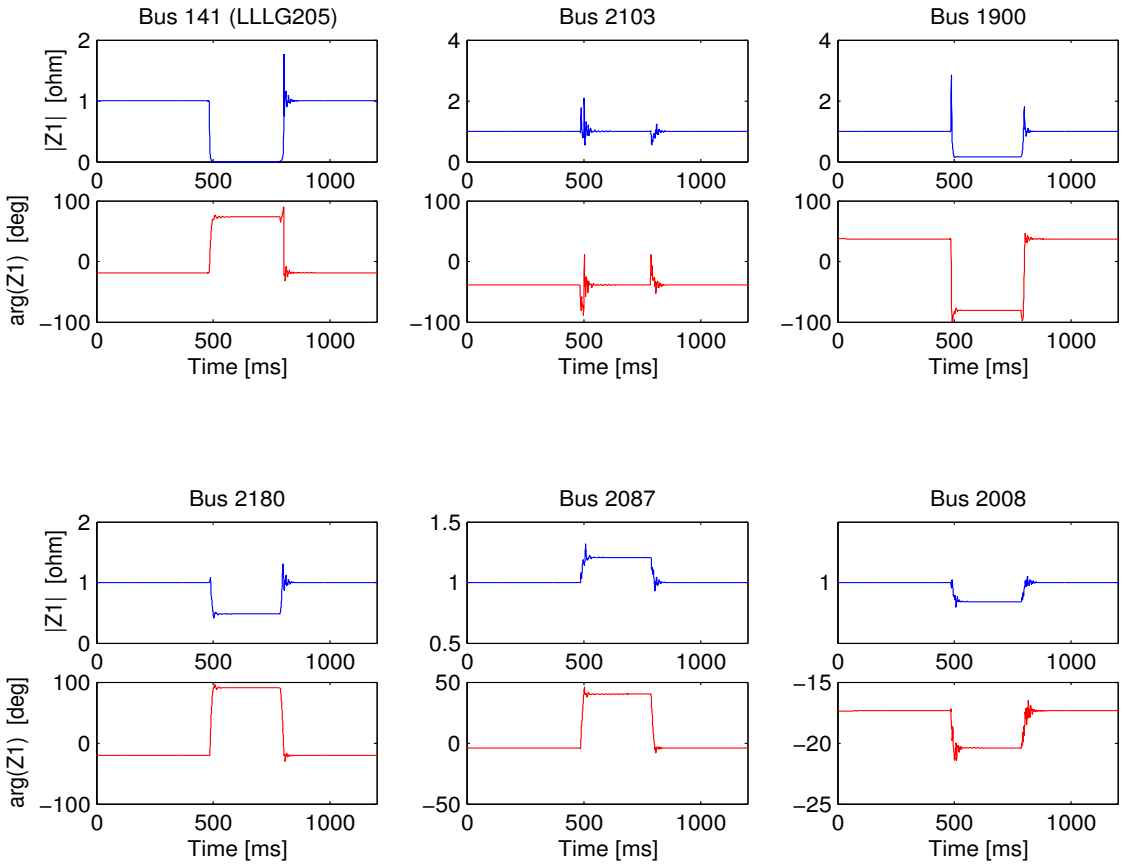

Figure 8: Positive sequence impedance and angle plot for LLLG fault at bus 205

In Figure 8 we see that at bus 2103 the during-sag impedance remains the same as the pre-sag impedance and its angle is negative indicating an upstream fault. At bus 2008 the during-sag impedance reduces and its angle is negative also indicating an upstream fault.

Figure 9 shows the distance relay method for a LLLG fault at bus 1922 i.e. downstream of bus 2103. In this case the during-sag impedance at bus 2103 reduces and its angle is positive indicating a downstream while at bus 2008 the during-sag impedance reduces and its angle is negative signifying an upstream fault.

Figure 10 below shows the distance relay method for a LLLG fault at bus 2015 i.e. downstream of bus 2008. In this case at bus 2008 the during-sag impedance reduces and its angle is positive indicating a downstream while at bus 2013 the during-sag impedance remains the same as pre-sag impedance and its angle is negative signifying an upstream fault.

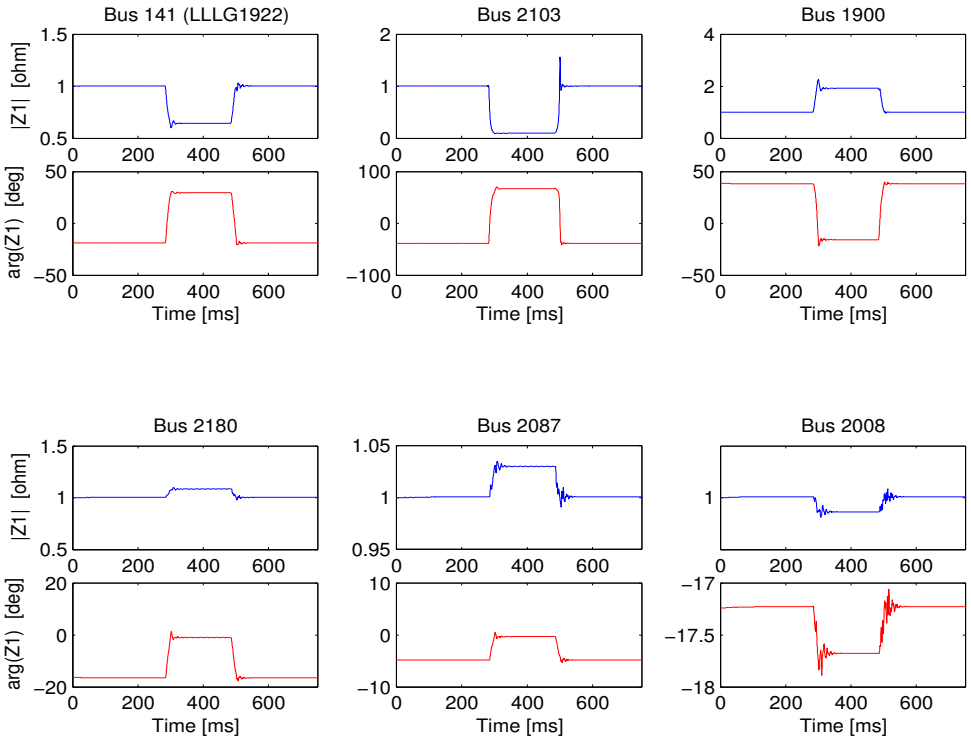

Figure 9: Positive sequence impedance and angle plot for LLLG fault at bus 1922

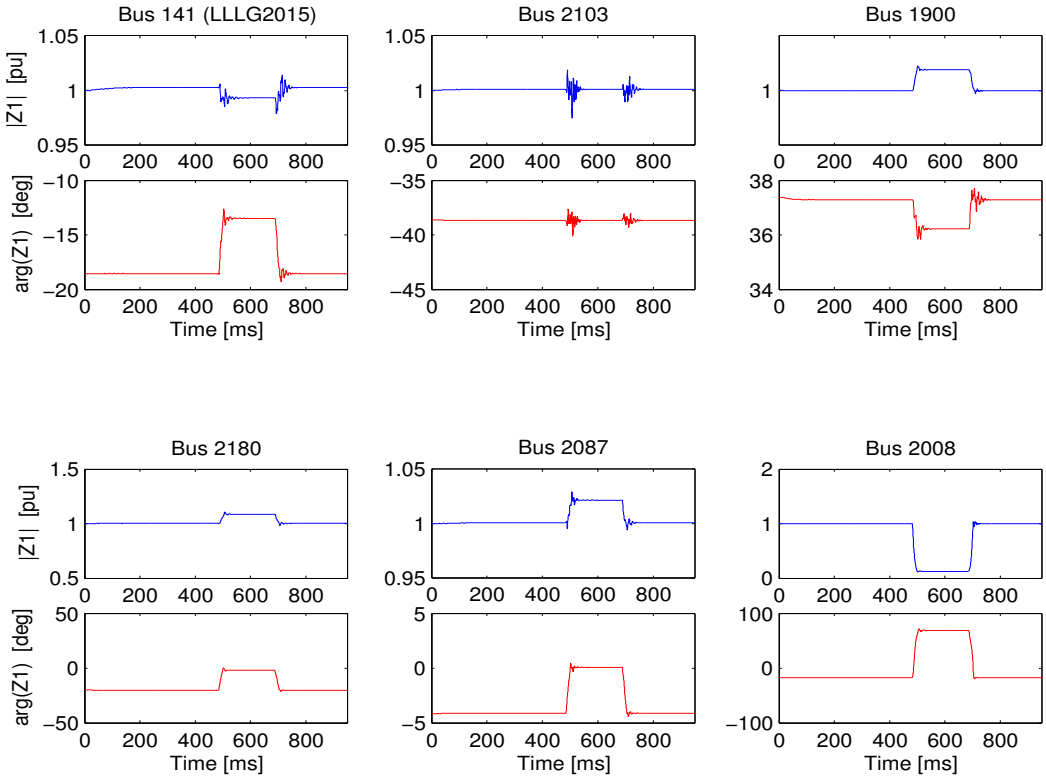

Figure 10: Positive sequence impedance and angle plot for LLLG fault at bus 2015

Figure 11 and Figure 12 show the response of the distance relay method to LG (phase A) and LLG (phases BC) faults at bus 205. The two monitoring locations still give correct sag source indication for each unbalanced fault. We see that at bus 2103 the during-sag impedance remains the same as the pre-sag impedance and its angle is negative indicating an upstream fault. At bus 2008 the during-sag impedance reduces and its angle is negative also indicating an upstream fault.

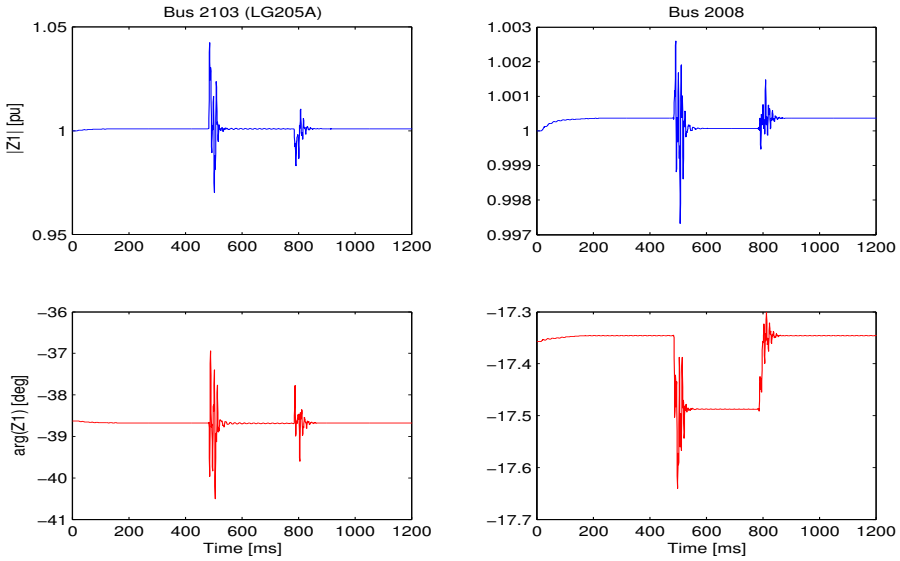

Figure 11: Positive sequence impedance and angle plot for LG fault at bus 205

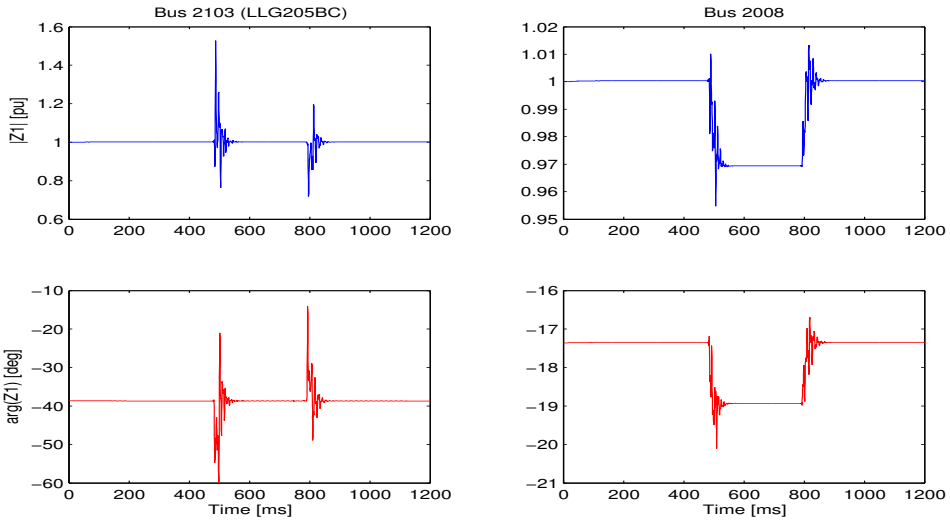

Figure 12: Positive sequence impedance and angle plot for LLG fault at bus 205

Figure 13 and Figure 14 depict results obtained with the distance relay method for LG (phase A) and LLG (phases BC) faults at bus 1922. The two monitoring locations still give correct sag source indication for each unbalanced fault. We see that at bus 2103 the during-sag impedance reduces and its angle is positive indicating a downstream fault while at bus 2008 the during-sag impedance reduces and its angle is negative indicating an upstream fault.

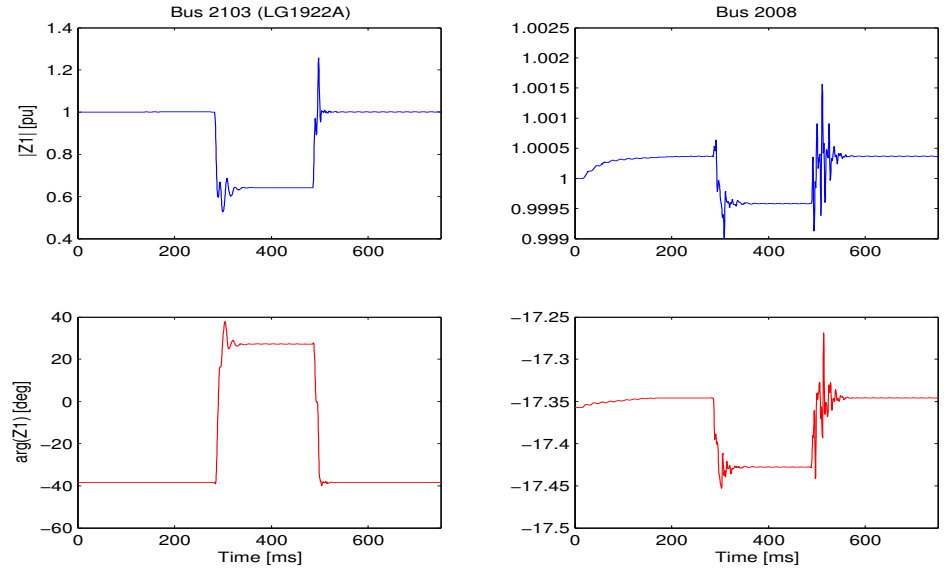

Figure 13: Positive sequence impedance and angle plot for LG fault at bus 1922

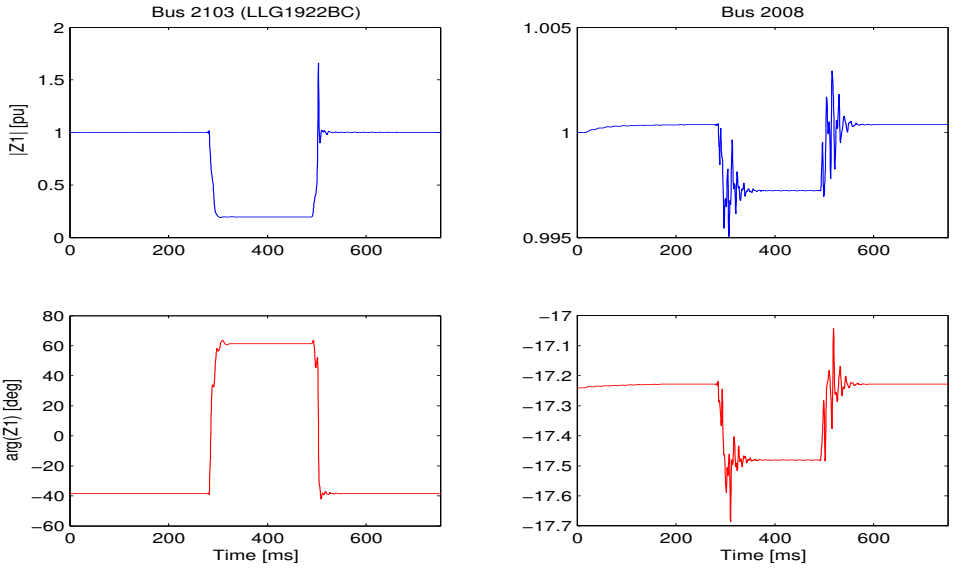

Figure 14: Positive sequence impedance and angle plot for LLG fault at bus 1922

Figure 15 and Figure 16 below show the response of the distance relay method to LG (phase A) and LLG (phases BC) faults at bus 2015. We again witness correct sag source indication at the two monitoring locations for the two unbalanced faults, upstream for bus 2103 and downstream for bus 2008.

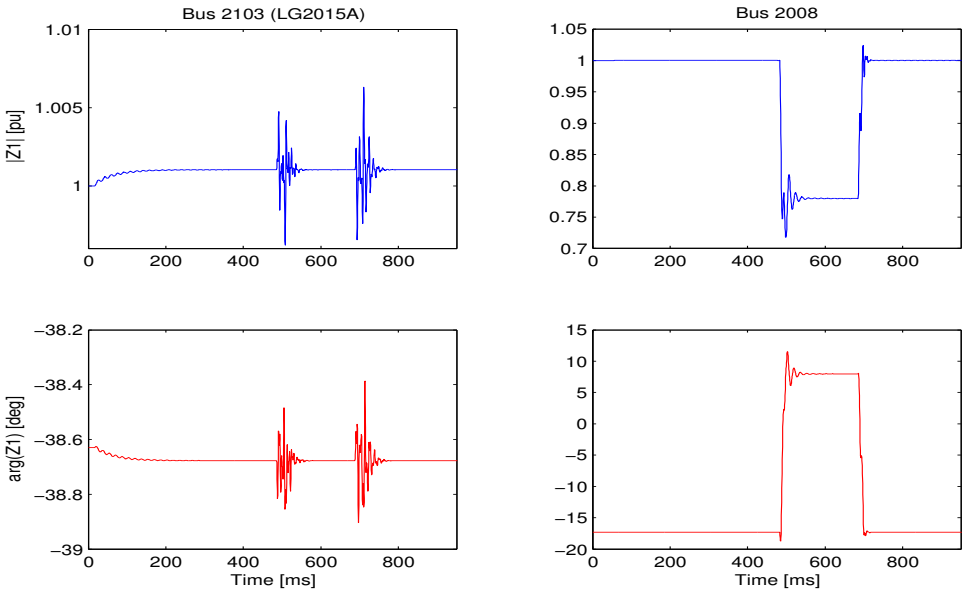

Figure 15: Positive sequence impedance and angle plot for LG fault at bus 2015

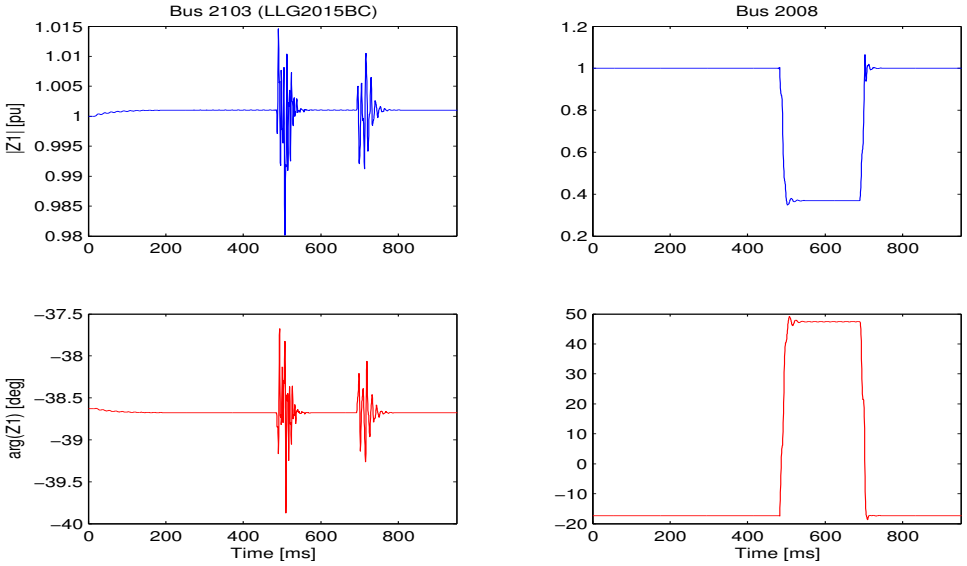

Figure 16: Positive sequence impedance and angle plot for LLG fault at bus 2015

The rest of the DR method results for simulations involving other fault types are given in appendix 1. Table 2 below gives a summary of the performance of the distance relay method.

Table 2: Summary of DR results

Fault Type	Monitor Position	
	Bus 2103	Bus 2008
LG205A	Upstream	Upstream
LLG205BC	Upstream	Upstream
LLLG205	Upstream	Upstream
LG1922A	Downstream	Upstream
LLG1922BC	Downstream	Upstream
LLLG1922	Downstream	Upstream
LG2015A	Upstream	Downstream
LLG2015BC	Upstream	Downstream
LLLG2015	Upstream	Downstream
LG2230A	Upstream	Upstream
LLG2230BC	Upstream	Upstream
LLLG2230	Upstream	Upstream

5.1.2 Slope of System Trajectory method applied to the Brazilian network

The Slope of System Trajectory has results of the location presented per phase. As mentioned in the features of the Brazilian network above the sag type is preserved on either side of the star-star transformer because of its grounding. We will use the faulted phase as the phase to give us the sag source direction. For LL(G) and LLL(G) faults this means the slopes in the affected phases have to give the same sign.

Presentation of graphs is such that the top layer gives results for the monitor at bus 2103 while the bottom layer indicates results for the monitor at bus 2008 for phase A, B and C respectively.

Figure 17 to Figure 23 below show the response of the SST method at bus 2103 and 2008 for LG, LLG and LLLG faults at buses 205, 1922, 2230 and 2015. As in the DR method the fault type is indicated on the top left subplot of each figure in brackets.

In Figure 17 the fault type is LG205A. This is interpreted as a line-to-ground fault at bus 205 in phase A. Therefore we use phase A as the phase to give the sag source direction. In this case we have a positive slope for the monitor at bus 2103 giving an upstream direction. The monitor at bus 2008 has a negative slope meaning a downstream sag source. However the actual sag source direction at bus 2008 for this fault is upstream. We shall come back to this issue later.

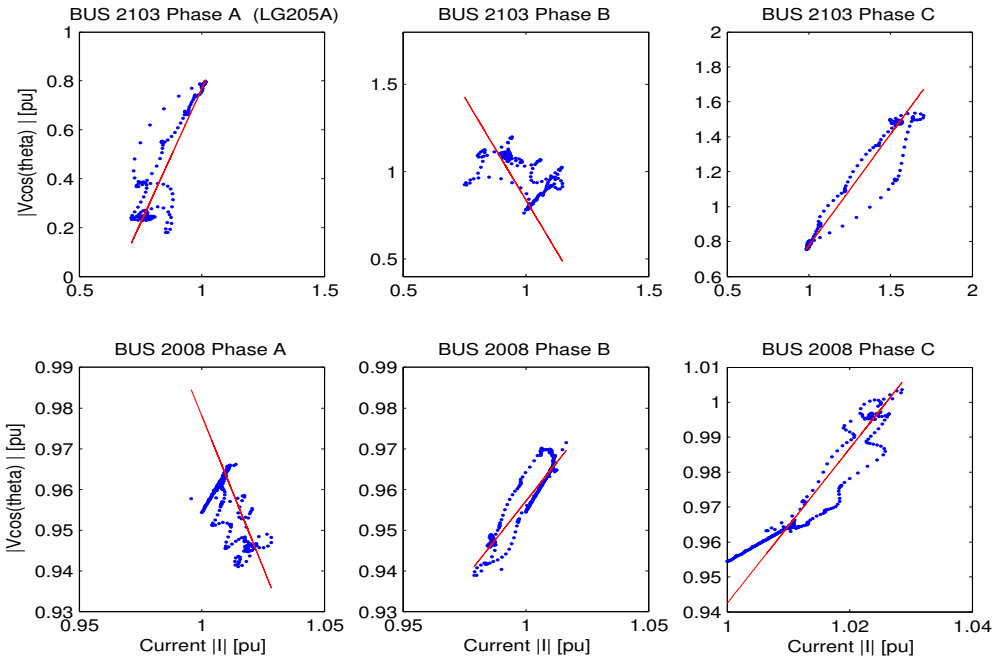

Figure 17: SST Method for LG fault at bus 205

In Figure 18 the fault type is LLG205BC and the faulted phases are B and C. These two phases give the same slope polarity for the monitor at bus 2103 indicating an upstream fault. At bus 2008 phase B and C give conflicting slope polarities and in such a case we are undecided as to the direction of the sag source. As before, we shall come back to this later.

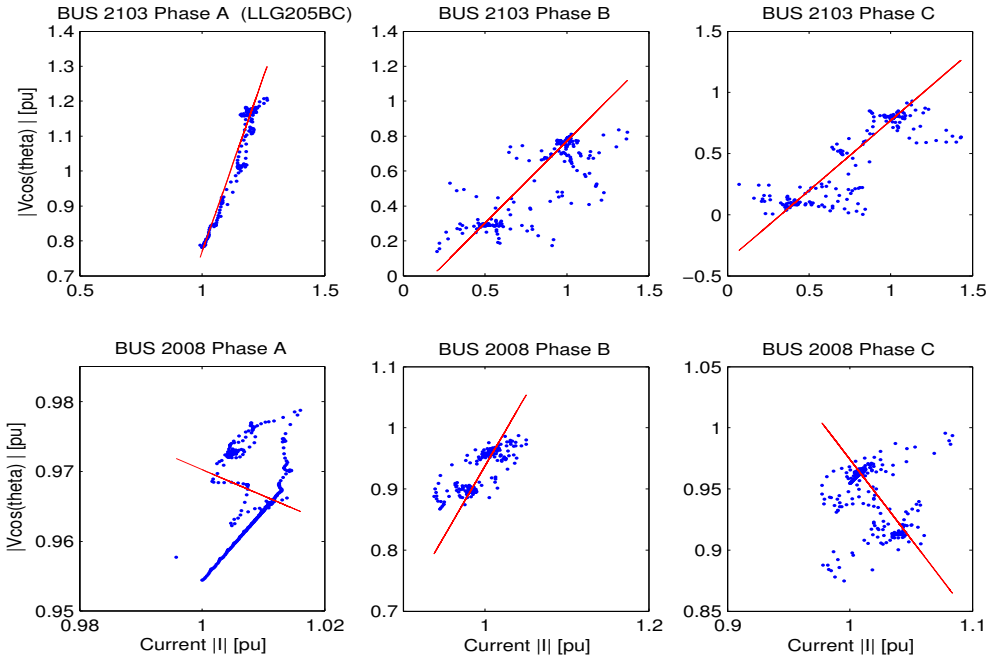

Figure 18: SST Method for LLG fault at bus 205

Figure 19 below is for a three-phase to ground fault at bus 205. As this is a balanced fault it is expected that the three phases should give identical slope polarities and any one of the phases can be used to give sag source direction. The monitor at bus 2103 conforms to this and indicates an upstream sag source while the monitor at bus 2008 has a negative slope in phase A and positive slopes in both phase B and C. Again this leads to an indecision. This will be explained later.

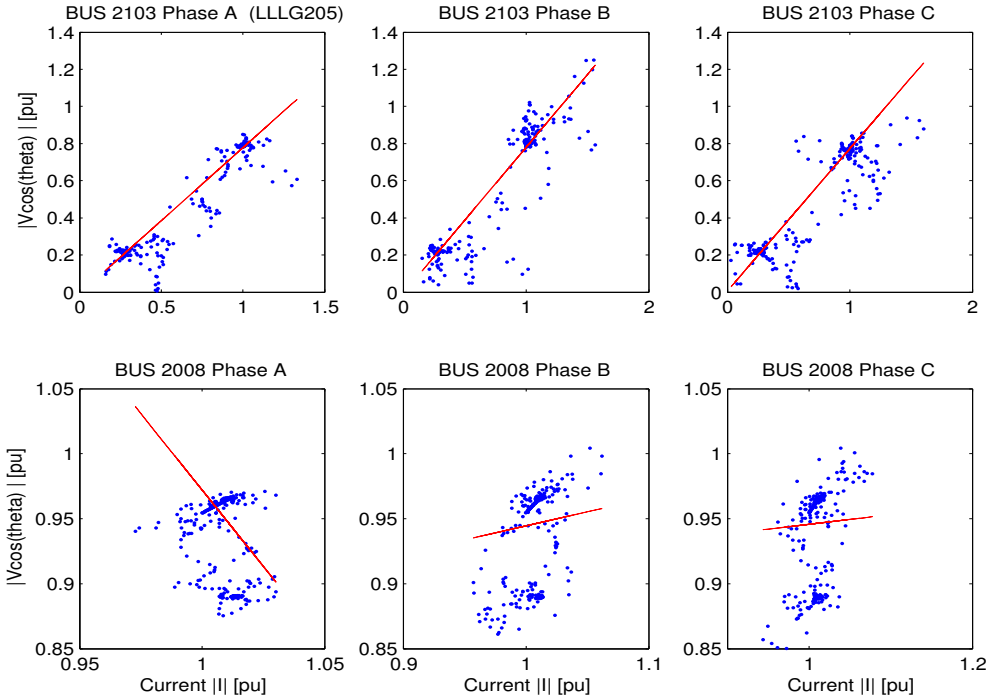

Figure 19: SST Method for LLLG fault at bus 205

Figure 20 shows a case where the two monitoring locations give correct sag source direction for a LLLG fault at bus 1922. This is downstream for the monitor at bus 2103 and upstream for the monitor at bus 2008.

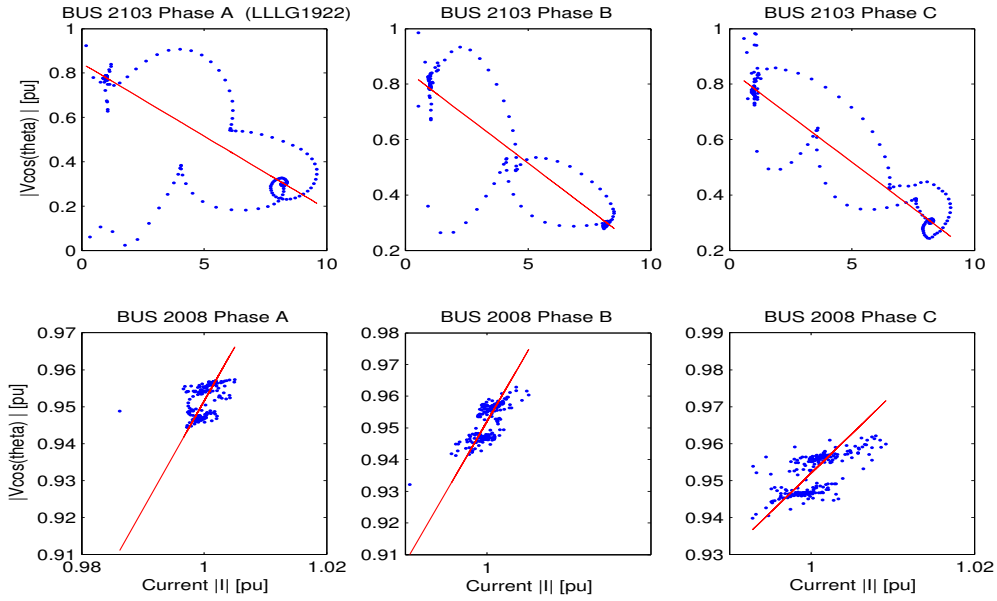

Figure 20: SST Method for LLLG fault at bus 1922

Figure 21 also shows a case where a LLG fault at bus 2015 is indicated correctly for both monitoring locations. At bus 2103 the monitor shows an upstream fault while at bus 2008 the monitor shows a downstream fault.

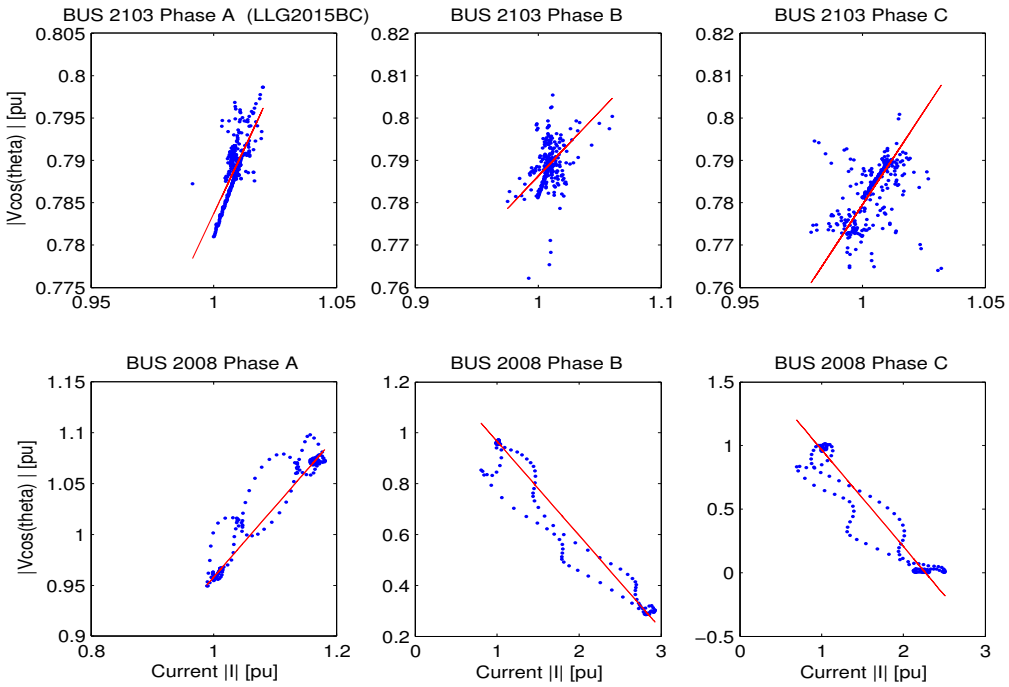

Figure 21: SST Method for LLG fault at bus 2015

Figure 22 below shows correct sag source direction (upstream) for the monitor at bus 2103 while the monitor at bus 2008 registers indecision for a LLG fault at bus 2230.

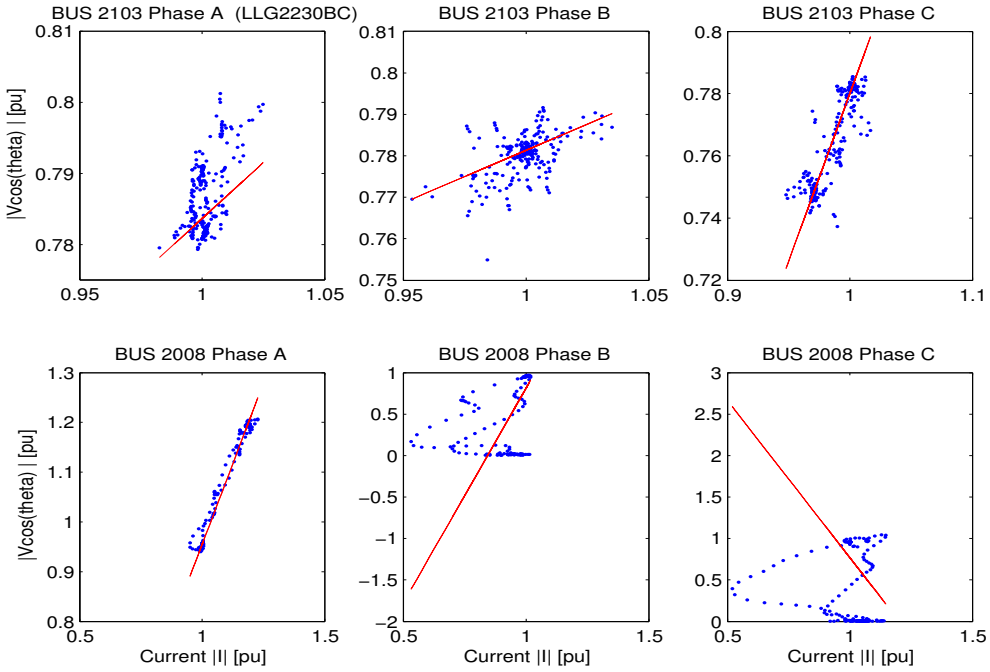

Figure 22: SST Method for LLG fault at bus 2230

In Figure 23 the fault type is LLLG2230. This is an upstream three-phase to ground fault for both monitoring positions. The monitor at bus 2103 correctly indicates an upstream sag source while the monitor at bus 2008 shows a downstream fault which is incorrect.

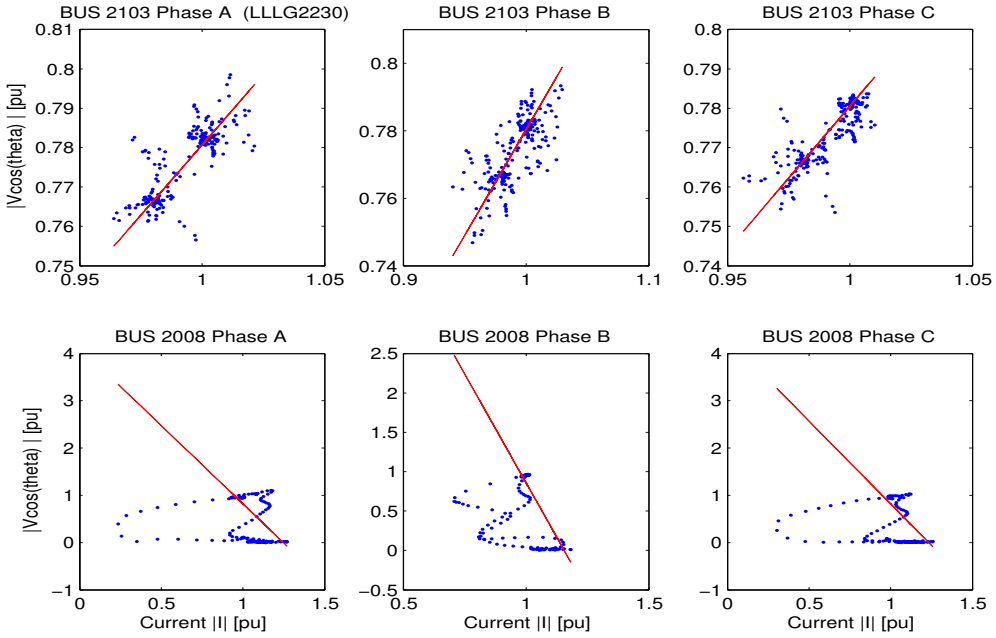

Figure 23: SST Method for LLLG fault at bus 2230

The reason for showing Figure 20 to Figure 23 will become evident once the cases of wrong sag source direction indication are analyzed.

Table 3 gives a summary of the response of the SST method for LG, LLG and LLLG faults simulated at buses 205, 1922, 2230 and 2015.

Table 3 : Summary of SST results

Fault Type	Monitor Position	
	Bus 2103	Bus 2008
LG205A	Upstream	Downstream (Wrong !)
LLG205BC	Upstream	Indecisive
LLLG205	Upstream	Indecisive
LG1922A	Downstream	Upstream
LLG1922BC	Downstream	Upstream
LLLG1922	Downstream	Upstream
LG2015A	Upstream	Downstream
LLG2015BC	Upstream	Downstream
LLLG2015	Upstream	Downstream
LG2230A	Upstream	Upstream
LLG2230BC	Upstream	Indecisive
LLLG2230	Upstream	Downstream (Wrong !)

In Table 3 it can be seen that the monitor at bus 2103 gives correct sag source direction in all cases whilst the monitor at 2008 gives correct sag source direction for faults at bus 1922 and bus 2015. For faults at bus 205 and bus 2230 the monitor at 2008 is either indecisive or gives a wrong direction except for fault type LG2230A where the indication is correct.

As mentioned above we now come back to the monitor at bus 2008 and see why it is indecisive or gives wrong sag source direction for certain faults. Fault types responsible for indecision and wrong direction indication were re-simulated but this time without co-generation at bus 840. The results are indicated in Figure 24 to Figure 28 below.

We now have the following results for the monitor at bus 2008:

- LG205A Upstream as shown in Figure 24
- LLG205BC Decisive and Upstream as shown in Figure 25
- LLLG205 Decisive and Upstream as shown in Figure 26
- LLG2230BC Decisive and Upstream as shown in Figure 27
- LLLG2230 Upstream as shown in Figure 28

Observe that in all these cases the monitor at bus 2103 still gives correct sag source direction as the corresponding previous fault types.

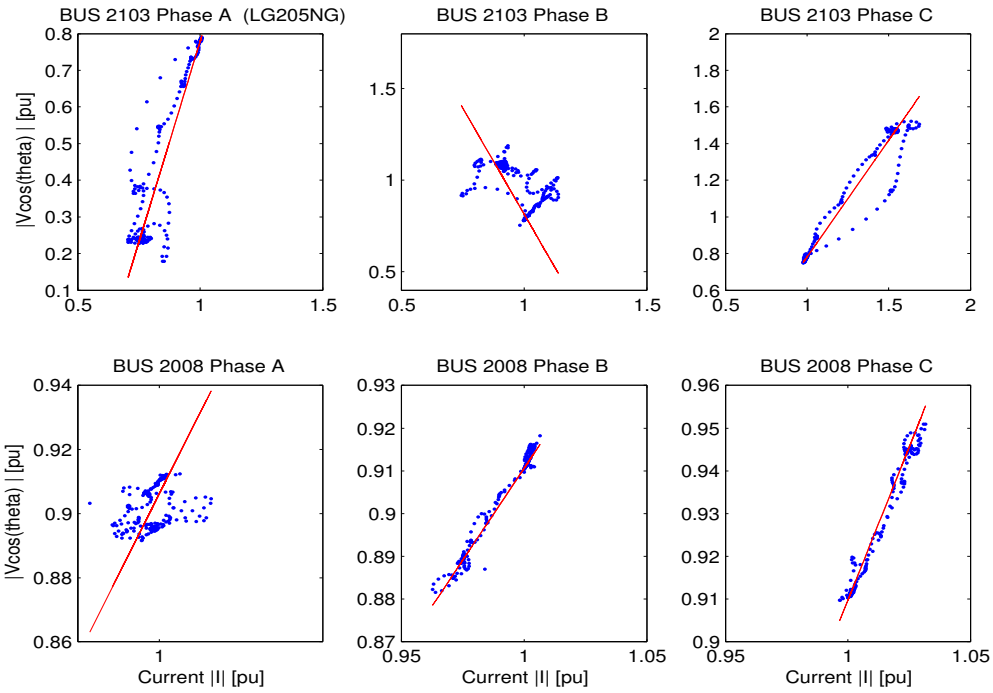

Figure 24: SST Method for LG fault at bus 205 (No generation at bus 840)

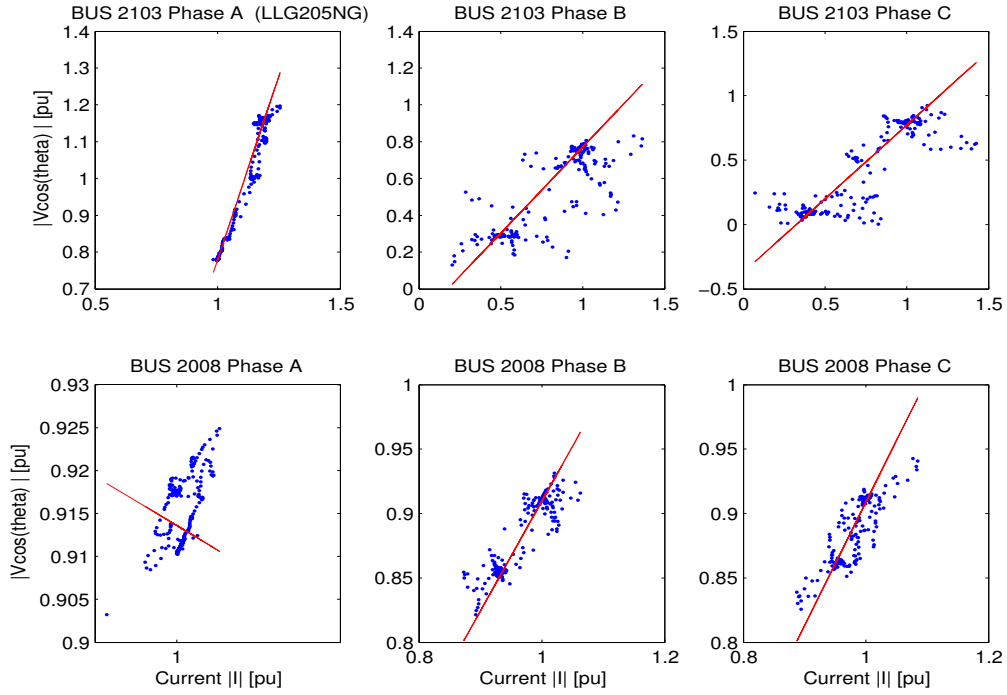

Figure 25: SST Method for LLG fault at bus 205 (No generation at bus 840)

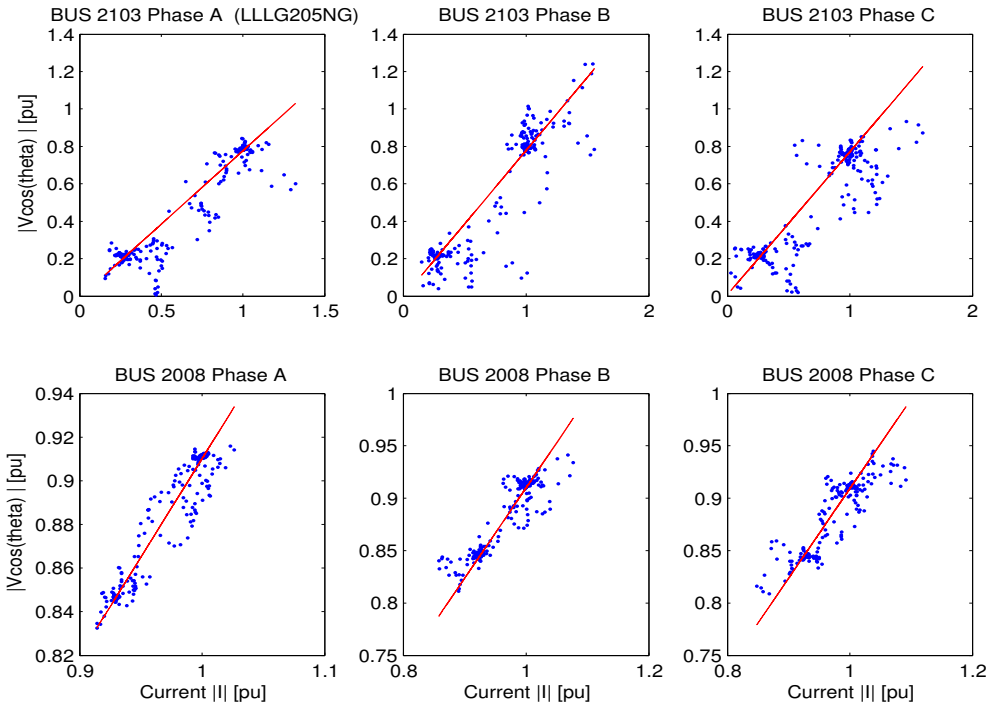

Figure 26: SST Method for LLLG fault at bus 205 (No generation at bus 840)

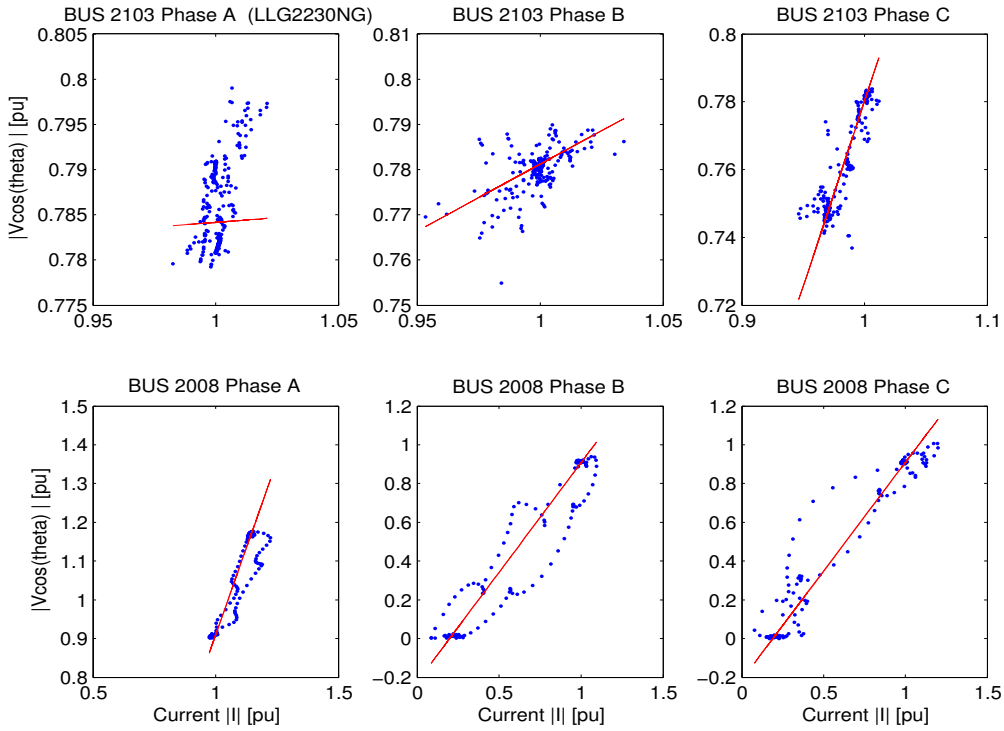

Figure 27: SST Method for LLG fault at bus 2230 (No generation at bus 840)

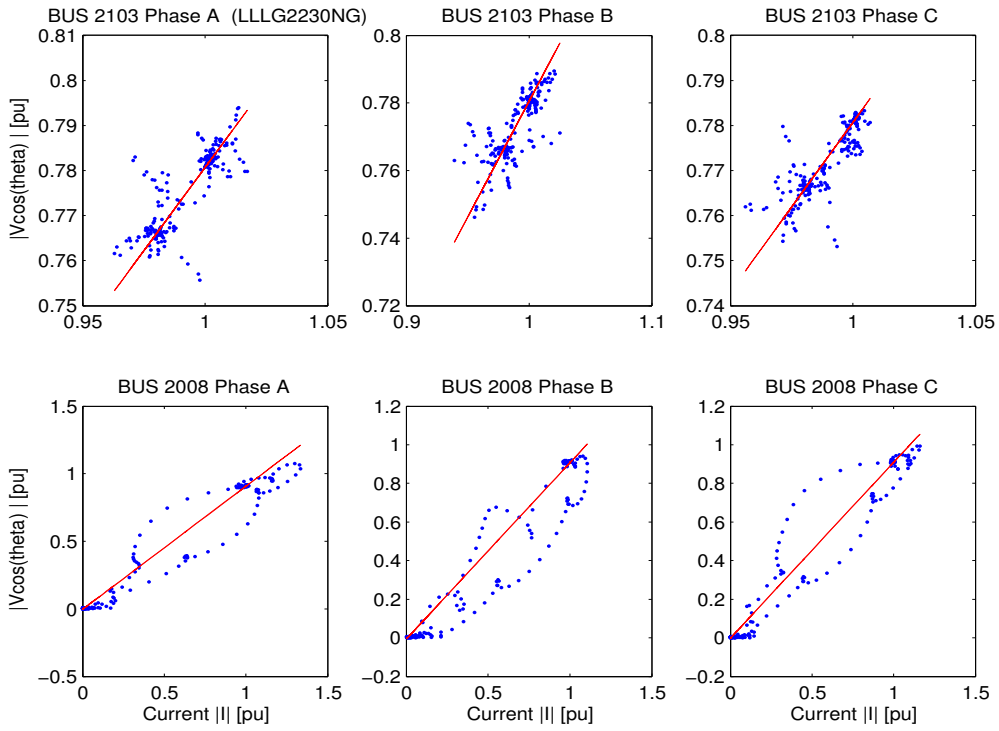

Figure 28: SST Method for LLLG fault at bus 2230 (No generation at bus 840)

We can therefore conclude that the generator at bus 840 works to mask the sag source direction for upstream faults which have a likelihood of reversing the direction of current flow at bus 2008. Faults at bus 2015 are not masked as the current contribution from the generator at bus 840 only flows to the fault at bus 2015 and does not result in reversal of current at bus 2008.

There is no contribution from the generator at bus 840 for remote faults such as those at bus 1922. Therefore such faults are indicated correctly at both buses 2103 and 2008.

The results observed at bus 2103 are expected to be affected if distributed generation is available downstream of this bus. This was confirmed by making simulations with the generator removed from bus 840 and placed at bus1783. The results obtained which are shown in Figure 29 to Figure 31 gave wrong sag source direction for faults on bus 205 and monitoring at bus 2103.

- LG205A Downstream as shown in Figure 29
- LLG205BC Downstream as shown in Figure 30
- LLLG205 Downstream as shown in Figure 31

This goes to further show the distributed generator influence.

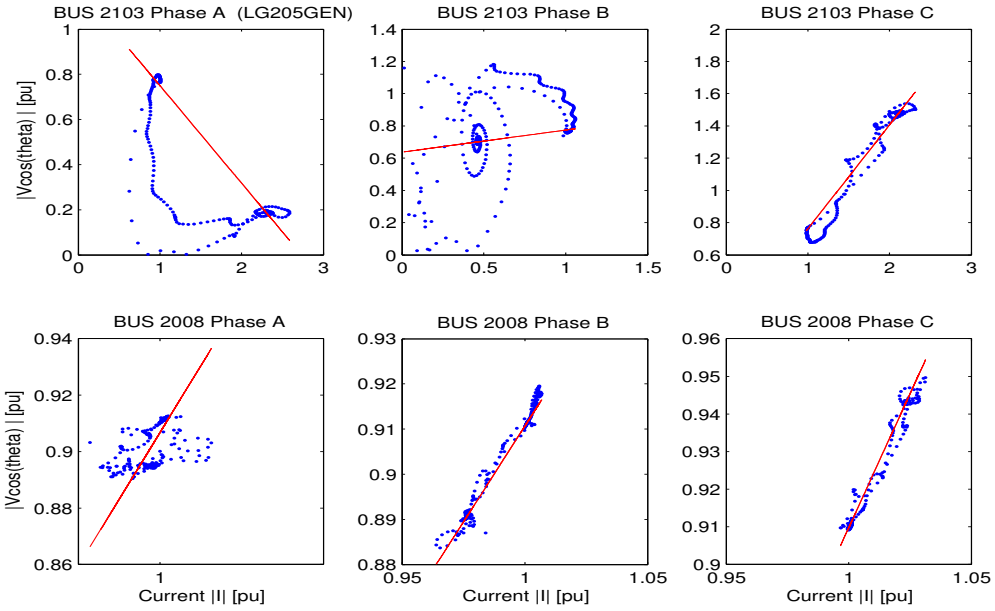

Figure 29: SST Method for LG fault at bus 205 (Generation moved from 840 to 1783)

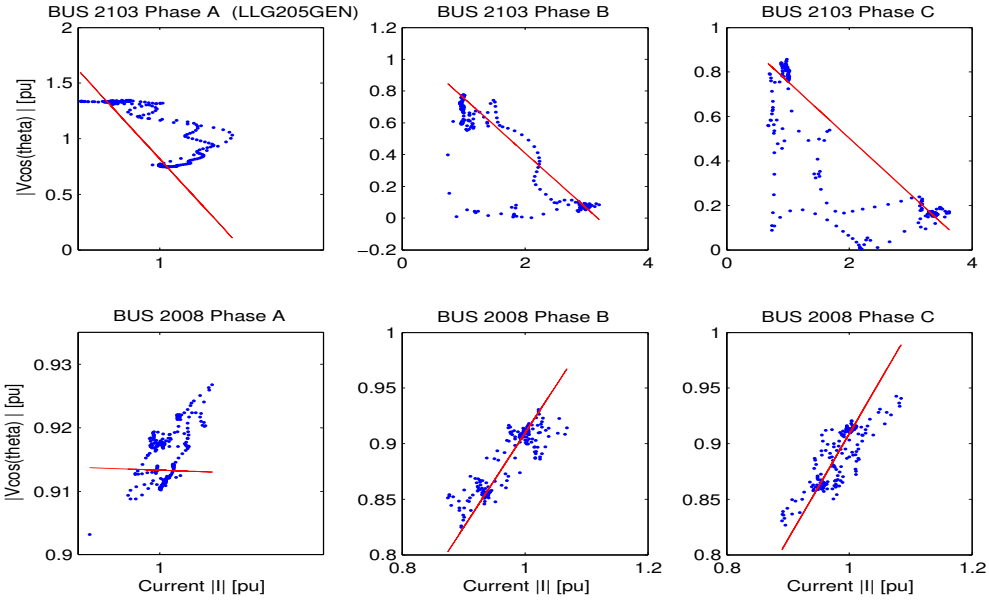

Figure 30: SST Method for LLG fault at bus 205 (Generation moved from 840 to 1783)

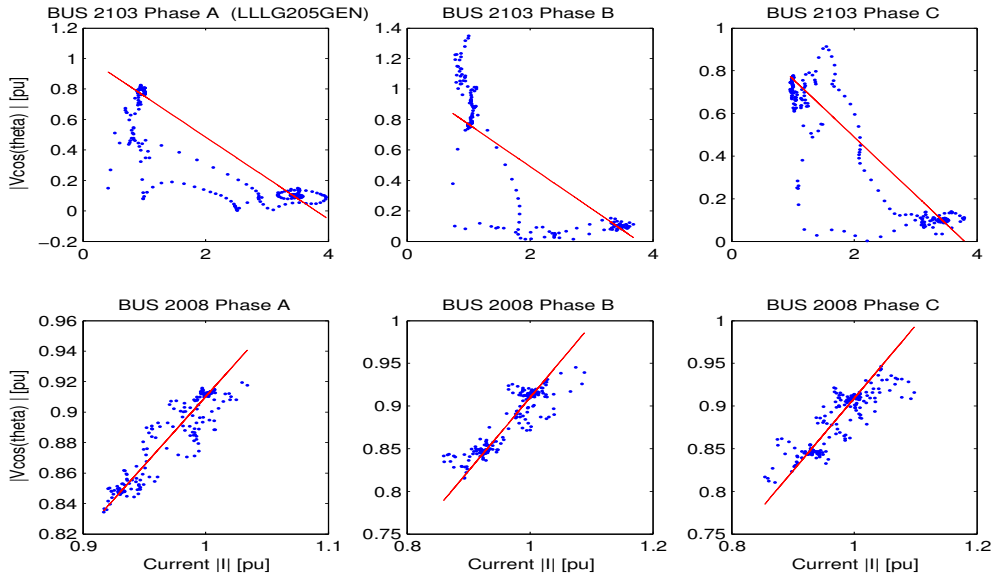

Figure 31: SST Method for LLLG fault at bus 205 (Generation moved from 840 to 1783)

Figure 33 and Figure 32 show how the presence or absence of distributed generation affects the sag magnitude (retained voltage) at bus 2008 for a LLLG fault at bus 2230. Without co-generation at beyond bus 2008 a sag due to a fault at bus 2230 is expected to propagate with the same magnitude to bus 2008. Figure 32 attests to this. However with co-generation at bus 840 the same fault type at bus 2230 yields a higher sag magnitude on the LV side than on the HV side of the transformer at bus 2230 as shown in Figure 33.

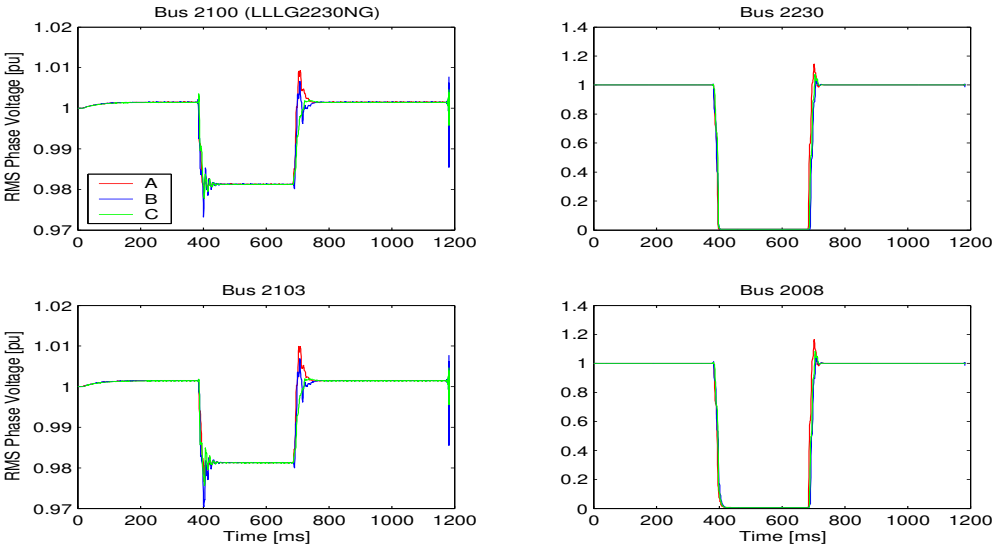

Figure 32: Dip magnitudes for LLLG fault at bus 2230 (without generation at bus 840)

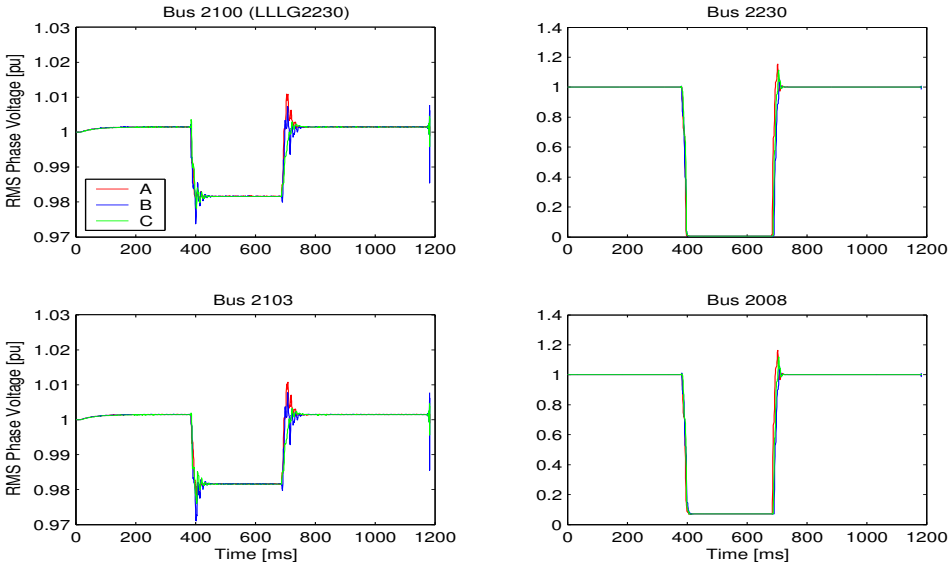

Figure 33: Dip magnitudes for LLLG fault at bus 2230 (with generation at bus 840)

5.1.3 Real Current Component method applied to the Brazilian network

The Real Current Component method (RCC) like the SST method also has results shown per phase as shown in Figure 34 to Figure 37. A similar approach of taking the faulted phase(s) to indicate the sag source direction would be adopted. For this method a during fault positive steady state polarity indicates a downstream fault while a during fault negative steady state polarity indicates an upstream fault.

Results are presented in the same fashion as in the SST method. Top layer for monitor at bus 2103 and bottom layer for monitor at bus 2008 with the same phase order. As before the fault type is indicated in brackets on the top left subplot.

Figure 34 shows the response or the RC method to a LG fault at bus 205 in phase A. It can be seen in this figure that the monitor at bus 2103 has a negative steady state during-fault polarity indicative of an upstream fault. The monitor at bus 2008 has a positive steady state during-fault polarity indicating a downstream fault. This is a wrong indication as the actual fault is upstream of bus 2008.

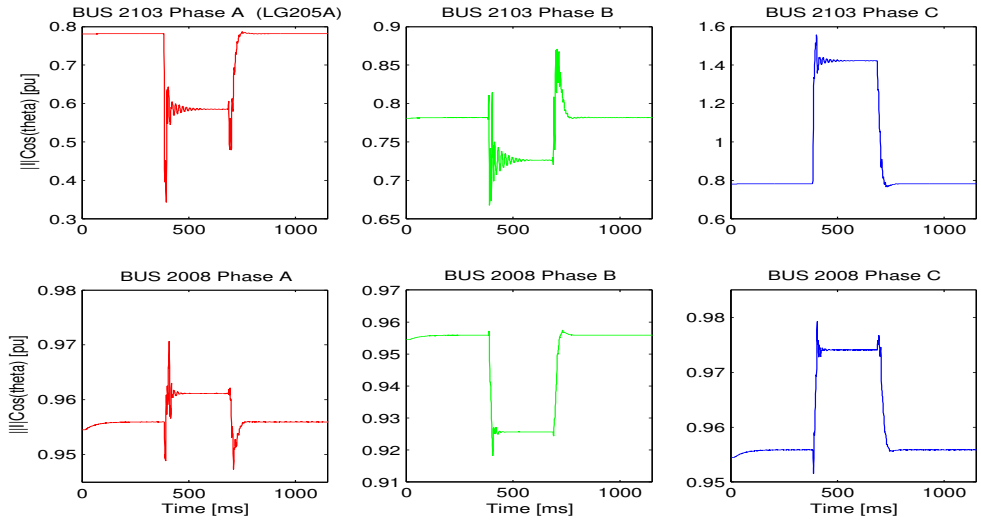

Figure 34: RCC Method for LG fault at bus 205

Figure 35 shows the response or the RC method to a LLLG fault at bus 205. In this case, all the three phases for both monitors show negative steady state during-fault polarity, correctly indicating that the fault is upstream of each monitor.

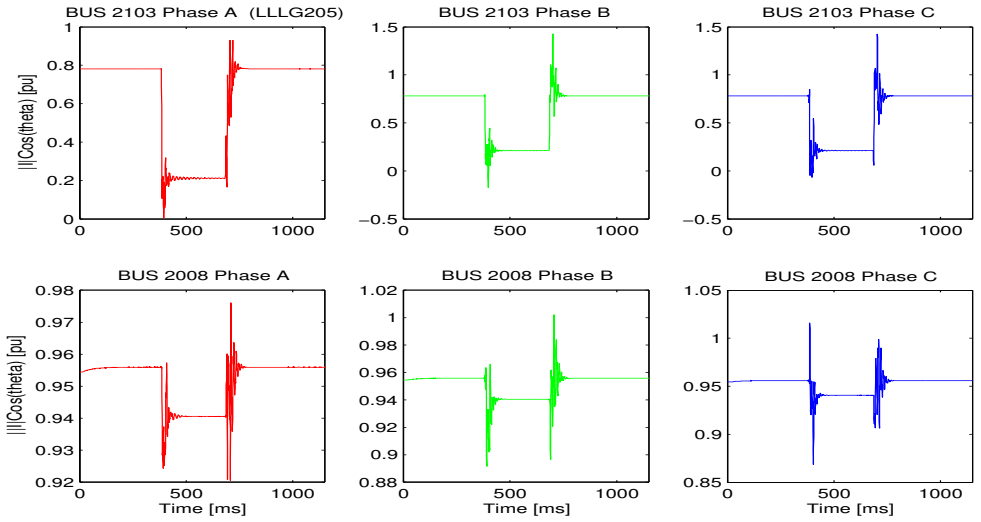

Figure 35: RCC Method for LLLG fault at bus 205

Figure 36 shows the case of a LLG fault in phases B-C downstream of bus 2103. At bus 2103 phases B and C give conflicting during fault steady state polarities and thus indecisive. The monitor at bus 2008 has negative polarities in both phase B and phase C indicating an upstream fault.

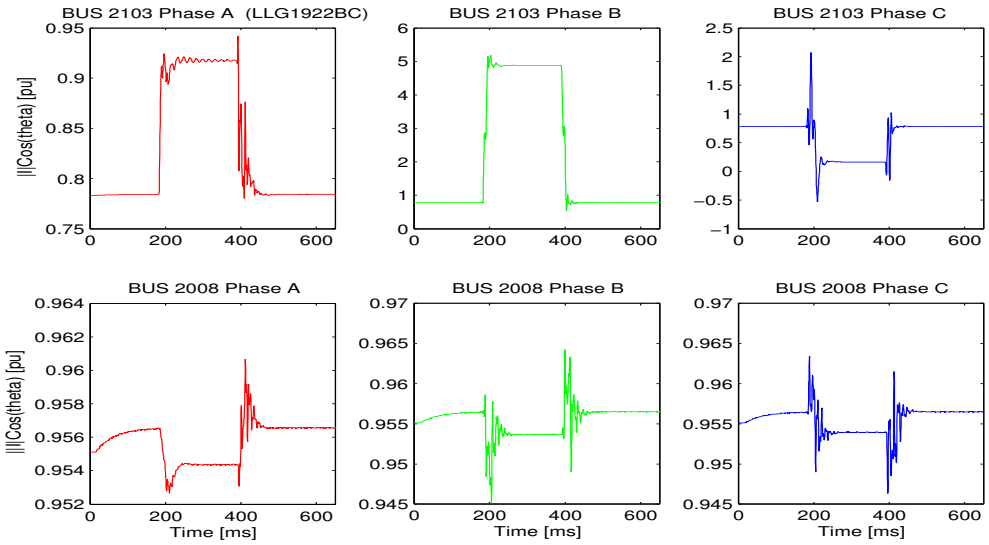

Figure 36: RCC Method for LLG fault at bus 1922

Figure 37 shows the case of a LG fault in phases A downstream of bus 2008. At bus 2103 phase A shows neither positive nor negative steady state deflection during the disturbance. This is also considered as being indecisive. The monitor at bus 2008 shows a positive steady state during-fault polarity showing a downstream fault.

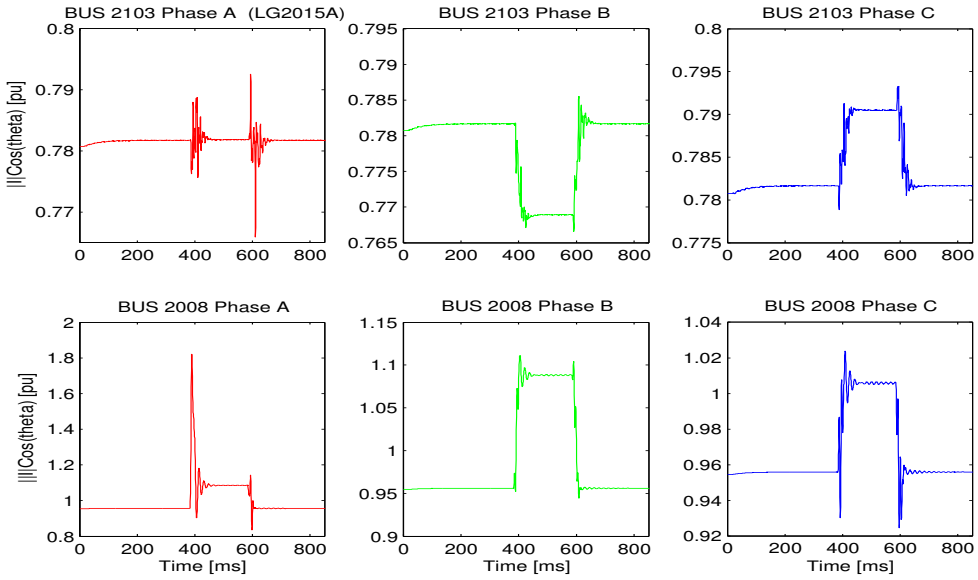

Figure 37: RCC Method for LG fault at bus 2015

Table 4 summarizes results for LG, LLG and LLLG fault simulations at bus 205, 1922, 2230 and 2015 for the RCC method. It can be seen in this table that the RCC method works well for balanced faults but its performance is not reliable for unbalanced faults.

Table 4 : Summary of RCC results

Fault Type	Monitor Position	
	Bus 2103	Bus 2008
LG205A	Upstream	Downstream (Wrong !)
LLG205BC	Upstream	Indecisive
LLLG205	Upstream	Upstream
LG1922A	Downstream	Downstream (Wrong !)
LLG1922BC	Indecisive	Upstream
LLLG1922	Downstream	Upstream
LG2015A	Indecisive	Downstream
LLG2015BC	Indecisive	Indecisive
LLLG2015	Upstream	Downstream
LG2230A	Upstream	Upstream
LLG2230BC	Indecisive	Upstream
LLLG2230	Upstream	Upstream

5.1.4 Reactive Power method applied to the Brazilian network

In Figure 38 and Figure 39 the two monitoring points are operating with negative reactive power in the pre-fault steady state. During the disturbance the reactive power for the monitor at bus 2103 increases but remains negative indicating an upstream fault. For the monitor at bus 2008 the reactive power becomes more negative also indicating an upstream fault.

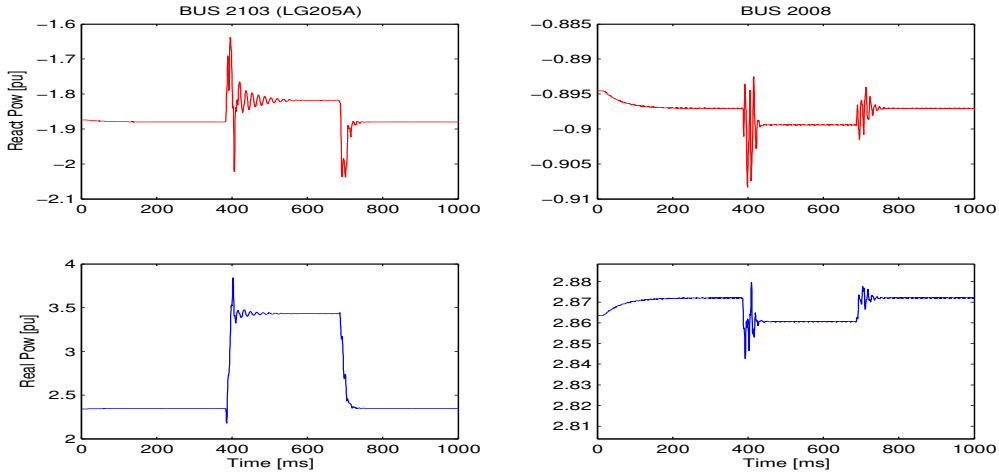

Figure 38: RP Method for LG fault at bus 205

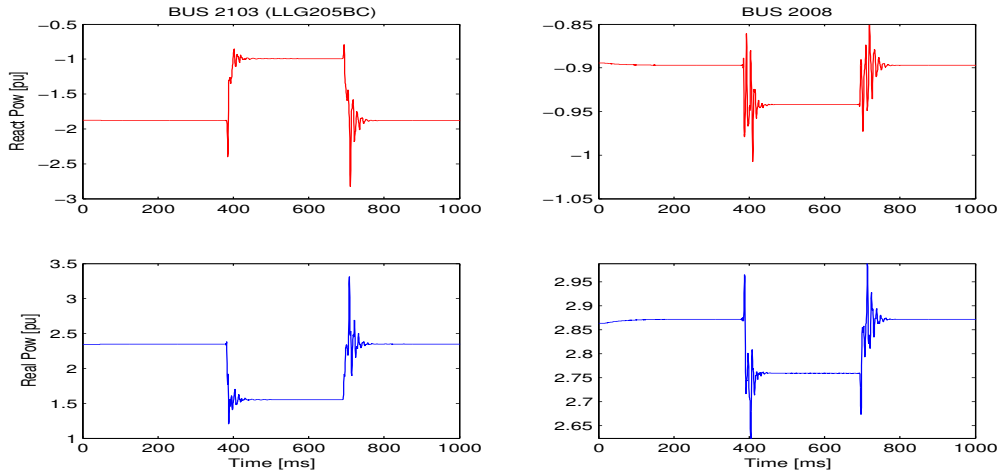

Figure 39: RP Method for LLG fault at bus 205

In Figure 40 the monitors at both buses again correctly indicate upstream sag source in each case. Observing Figure 38 to Figure 40 closely we note that the increase or decrease in reactive power is proportional to the severity of the sag (in energy level terms), lowest for LG faults and highest for LLLG faults. This pattern is consistent for the other graphs from Figure 41 to Figure 46.

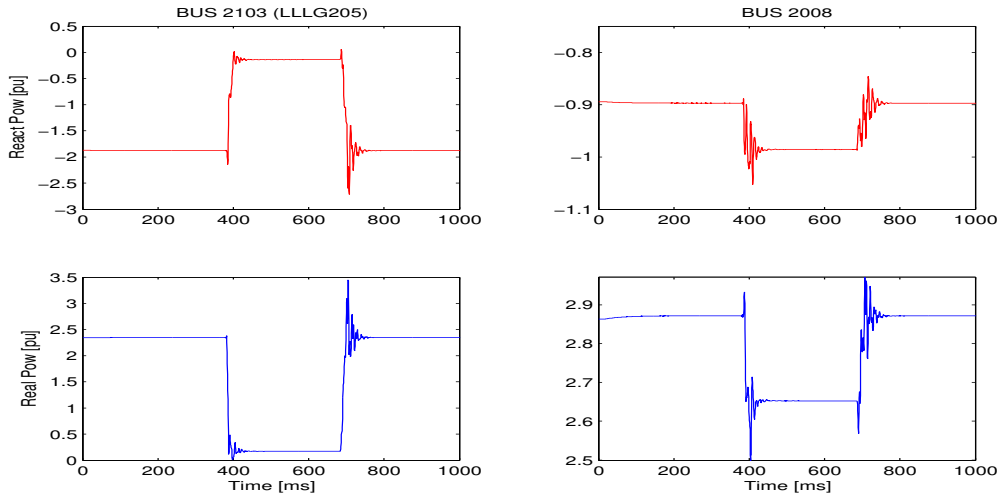

Figure 40: RP Method for LLLG fault at bus 205

Figure 41 to Figure 43 show reactive power plots for LG, LLG and LLLG faults downstream of bus 2103. These plots show that at bus 2103 the value of reactive power increases from negative pre-fault steady state value to a positive during fault steady state value signifying downstream faults. For the monitor at bus 2008 the during-fault reactive power value becomes more negative than the pre-fault value indicating upstream faults for all the three fault types.

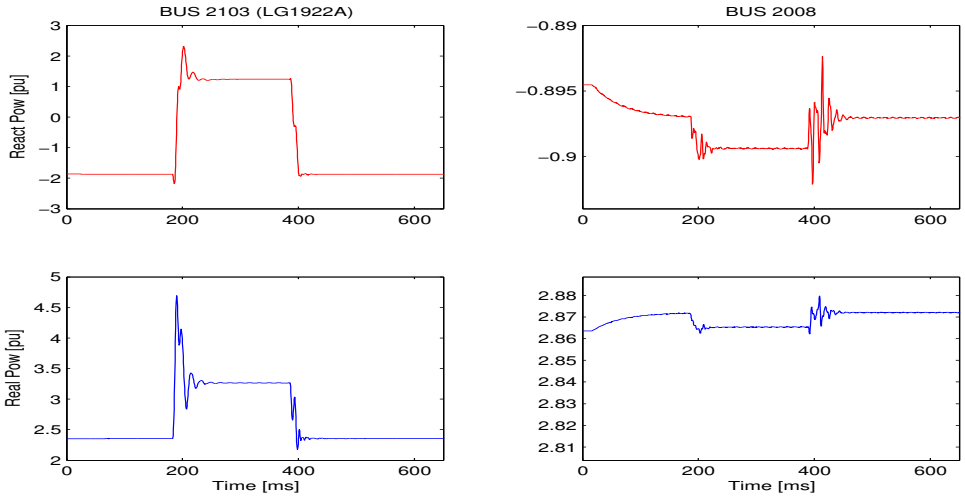

Figure 41: RP Method for LG fault at bus 1922

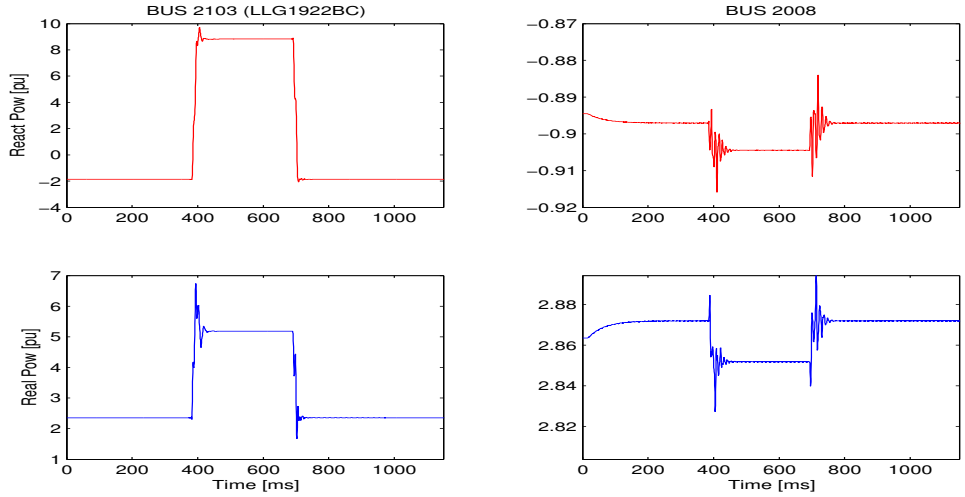

Figure 42: RP Method for LLG fault at bus 1922

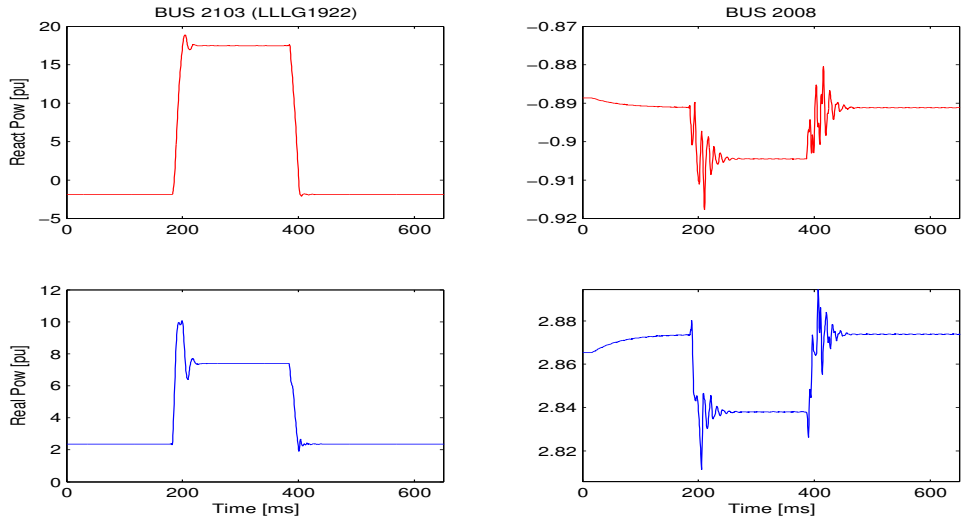

Figure 43: RP Method for LLLG fault at bus 1922

Figure 44 to Figure 46 reactive power plots for LG, LLG and LLLG faults downstream of bus 2008. Figure 44 shows negative during-sag steady state reactive power at bus 2103 thus correctly indicating an upstream fault. The monitor at bus 2008 also shows negative during-fault steady state reactive power signifying an upstream fault. However in this case the sag source direction is indicated wrongly.

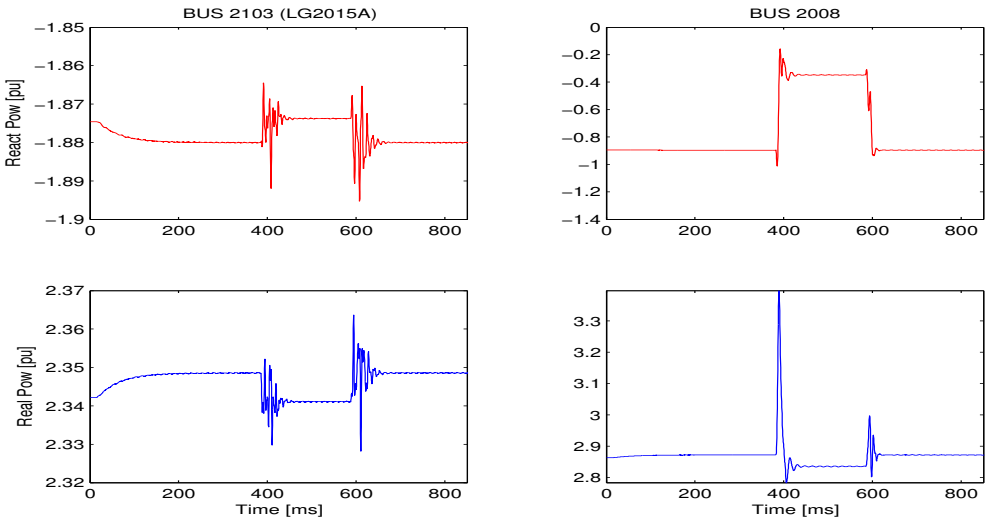

Figure 44: RP Method for LG fault at bus 2015

Both Figure 45 and Figure 46 show that at bus 2103 the during-fault steady state reactive power remains negative giving upstream sag sources while at bus 2008 the reactive power changes from a negative pre-fault value to a positive during-fault steady state value indicating downstream sag sources.

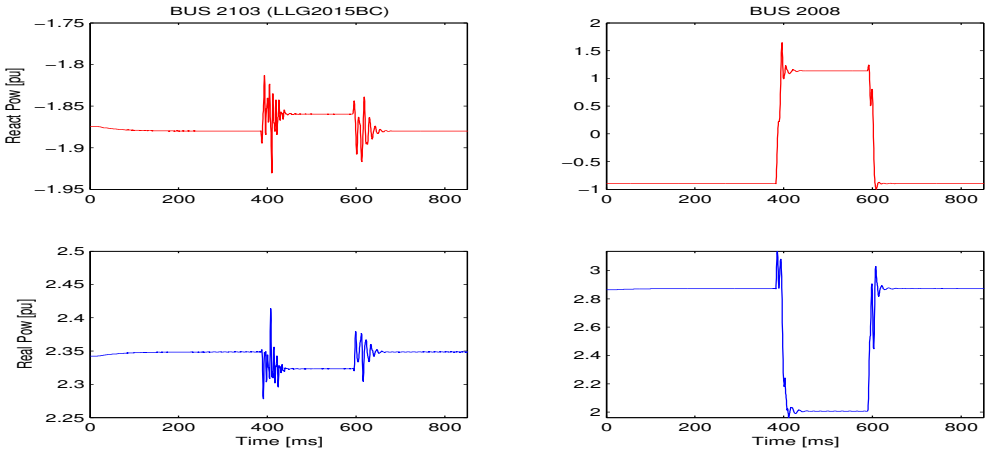

Figure 45: RP Method for LLG fault at bus 2015

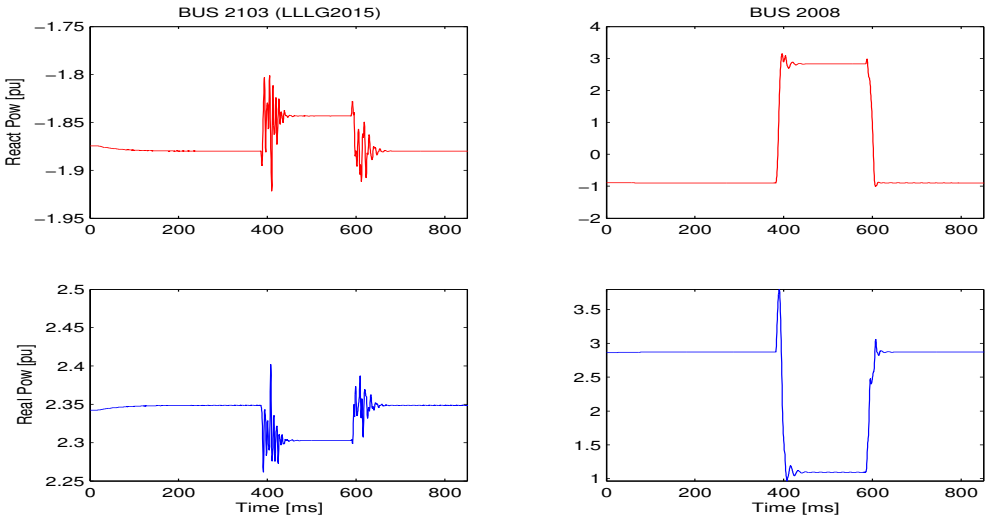

Figure 46: RP Method for LLLG fault at bus 2015

Table 5 summarizes results of the reactive power method for LG, LLG and LLLG fault simulations at bus 205, 1922, 2230 and 2015 respectively. In this table the sag sources are indicated correctly for all faults except for LG2015A where the monitor at bus 2008 gives a wrong indication.

Table 5 : RP method results summary

Fault Type	Monitor Position	
	Bus 2103	Bus 2008
LG205A	Upstream	Upstream
LLG205BC	Upstream	Upstream
LLLG205	Upstream	Upstream
LG1922A	Downstream	Upstream
LLG1922BC	Downstream	Upstream
LLLG1922	Downstream	Upstream
LG2015A	Upstream	Upstream (Wrong!)
LLG2015BC	Upstream	Downstream
LLLG2015	Upstream	Downstream
LG2230A	Upstream	Upstream
LLG2230BC	Upstream	Upstream
LLLG2230	Upstream	Upstream

Table 6 shows a summary of the performance of the four location methods for eleven fault types simulated at each of the following buses: 1922, 2100, 205, 2015, 2230 and 1933. This means that each of the four methods had to be tested for 66 (11x6) fault types. For the SST method a correction is made for two cases where the direction was wrongly indicated. This is because active power reversal was detected.

Table 6: location methods performance in Brazilian network

FAULT TYPE	BUS 2103 PERFORMANCE [%]				BUS 2008 PERFORMANCE [%]			
	DR	RP	SST	RCC	DR	RP	SST	RCC
Balanced	100	100	100	100	100	100	91.67	91.67
Unbalanced	100	100	100	66.67	100	94.4	61.1	46.3

Results for the distance relay method and reactive power method which do not present outputs on a per phase basis can be grouped. For example simulating a LG fault at a particular point in phase A, B and C would give the same value of during sag impedance and angle. Similarly for LL and LLG faults simulating in phase AB, BC or CA doesn't really matter so much as the results would be identical. A LLL fault and LLLG fault would also give the same results.

For the methods presenting results per phase simulations in different phases or phase combinations would produce different results. For the slope of system trajectory method one has to check for the possibility of current reversal when analyzing the results.

Comparing the performance of the location methods as summarized in Table 6 the DR, SST and RP methods are recommended for assessment in the Zambian grid.

5.2 Simulations in the Zambian Network

Indeni Petroleum Refinery is Zambia's sole crude oil process factory. One of its critical induction motors often trips on undervoltage and causes loss of the entire process. As a result of this the plant goes into chaotic shutdown. With chaotic shutdown there is material wastage and the restoration process usually takes several hours. Once operations at the factory are affected there is a risk of countrywide fuel shortages. This has a crippling effect on various sectors of the economy with the transport industry being most affected.

Power is handled by basically two utilities before getting to Indeni (CEC and Zecso). Figure 47 is a reduced network where the 330kV and 220kV networks are not shown. In this figure category 1 is the Indeni network. Category 2 to 4 belongs to Zesco while category 5 to 7 belongs to CEC. It is therefore crucial to locate the sources of sags so as to devise mitigation methods and allocate responsibilities to the parties involved.

The network of Figure 47 was modeled in PSCAD/EMTDC. Due to limitations on the number of nodes in the Student version of PSCAD/EMTDC the 3 x 220/66kV transformers at Maposa were represented as one transformer, so were the 3 x 66/33kV at Skyways. Voltage and current monitoring were done at Maposa66, Skyways66, Skyways33, Indeni 33A, and Indeni 33B. Only voltage signals were recorded at Indeni 6A and Indeni 6B.

The features of this network are;

- Single source (thus radial)
- Presence of Dy transformers to assess location methods when dip type changes
- Linear loads

Four types of faults (LG, LL, LLG and LLLG) were simulated at various buses for each of the following network categories.

1. Internal (Indeni) network. These are faults within the Indeni network on 6kv and 400V.
2. The two 33kV overhead lines directly feeding Indeni
3. Adjacent 33kV lines from Skyways Substation
4. 11kV lines after 33/11kV transformers at Skyways
5. 66kV lines from Maposa into Skyways
6. 66kV Maposa – Luanshya system
7. Upstream from Maposa 66kV.

Table 7 below summarizes the lowest dip magnitudes obtained at Indeni 6kV buses for each of the above seven fault categories. The dip magnitude at Indeni 6kV buses is of great importance because the main sensitive load is connected at this bus.

In Table 7 for rows with two values in a cell the top one represents the dip magnitude experienced at Indeni 6kV bus A whilst the bottom one represents the dip magnitude at

Indeni 6kV bus B. Further if the value is in brackets it indicates the faulted bus and is the dip experienced if the protection on that circuit does not operate as intended.

Rows showing only one value in a cell mean that the same dip magnitude was experienced at both Indeni 6A and Indeni 6B buses.

For internal faults (category 1) the lowest dip magnitude caused on one 6kV bus by faults from the other 6kV system is 0.88 pu. Faults on the 400V system do not threaten the operation of the sensitive motors connected on the 6kV buses as the worst dip magnitude to be experienced is 0.98 pu.

Faults in category 2 give a lowest dip magnitude of 0.18 pu. This is as a result of LL(G) or LLLG faults on either line near the Indeni 33kV boards.
Category 3 faults yield dip magnitudes of 0.7 pu for LG faults and 0.25 – 0.3 pu for LL and LLLG faults. Direct faults on the 33kV busbar at Skyways also result in dip magnitudes of 0.7 pu for LG faults and 0.02 – 0.03 pu for LL(G) or LLLG faults respectively.

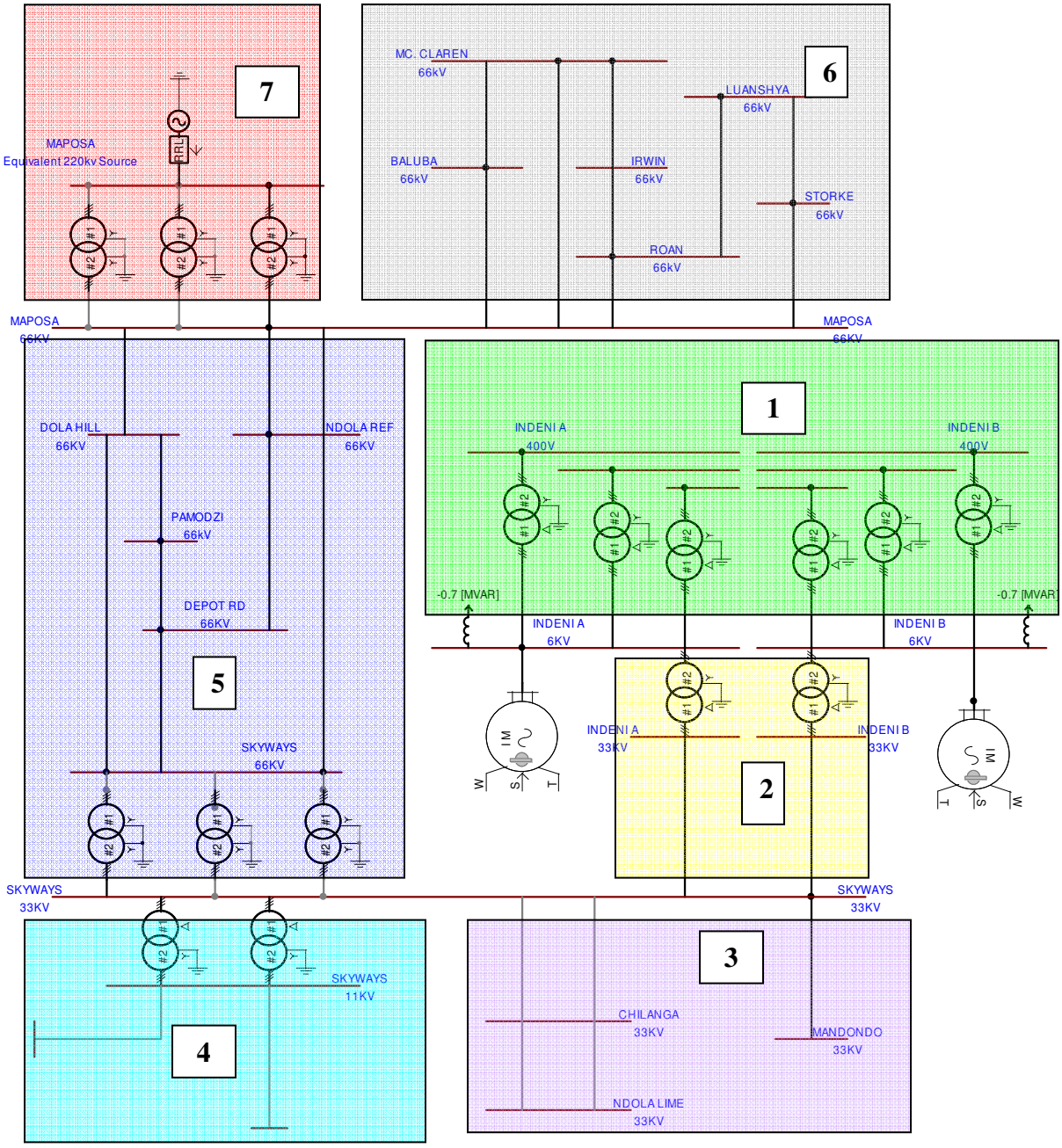

Figure 47: Network Fault Categories – Zambian Grid

Category 4 faults directly on the 11kV bus at Skyways give dip magnitude of 0.4 pu for LG faults and 0.32 pu as worst case for LLLG faults. Faults on a remote 11kV bus (about 8km away from Skyways) yield dip magnitudes of between 0.6 – 0.7 pu for all fault types.

Category 5 faults give a worst dip of 0.15 pu for LL or LLLG faults at Ndola Refinery and an upper dip magnitude of 0.8 pu for a LG fault at Dola Hill.

Category 6 faults yield dip magnitudes of around 0.73 pu as lowest and 0.94 pu as highest.

Table 7: Dip magnitude at Indeni 6 kV buses for different fault categories

Category	Faulted Bus	Dip Magnitude at Indeni 6kV Buses [pu]			
		LG	LL	LLG	LLLG
1	Indeni 6A	(0.12) 0.92		(0.12) 0.90	(0.12) 0.88
	Indeni 6B	0.92 (0.12)		0.90 (0.12)	0.88 (0.12)
	Indeni T8 400V	0.997 0.984		0.997 0.98	0.995 0.98
	Indeni T10 400V	0.997 0.984		0.997 0.98	0.995 0.98
	Indeni T7 400V	0.984 0.997		0.98 0.997	0.98 0.995
	Indeni T5 400V	0.984 0.997		0.98 0.997	0.98 0.995
2	Indeni 33A	(0.68) 0.74		(0.04) 0.18	(0.04) 0.18
	Indeni 33B	0.74 (0.68)		0.18 (0.04)	0.18 (0.04)
3	Ndola Lime	0.7	0.3	0.3	0.3
	Chilanga	0.7	0.25	0.25	0.25
	Skyways33	0.7	0.02	0.03	0.03
4	Skyways11	0.40	0.52	0.37	0.32
	Remote 11kV Sub	0.69	0.70	0.65	0.60
5	Dola Hill	0.80	0.33	0.33	0.31
	Depot Road	0.77	0.30	0.30	0.30
	Ndola Ref	0.73	0.15	0.15	0.15
6	Mc Claren	0.92	0.73	0.73	0.73
	Roan	0.93	0.78	0.78	0.78
	Luanshya	0.94	0.82	0.82	0.82
7	Maposa 66kV	0.57	0.01	0.01	0.01

Considering that LG faults are the most common on the power system we can summarize the lowest dip magnitudes experienced on Indeni 6kV buses due to these faults as shown in Table 8.

The value shown in brackets for category 4 is due to a LG fault in the substation. The other value is as a result of a LG fault on an 11kV bus 8km away from the substation (typical lengths for distribution feeders).

The region of vulnerability for sensitive loads connected on the Indeni 6kV buses is as a result of faults in network categories 2, 3, 4, 5 and 7. Category 1 network is solely underground cable and may not have a high frequency of fault occurrence as overhead lines.

Table 8: 6kV Dip magnitude caused by LG faults [pu]

Category	I	II
1	0.92	0.92
2	0.74	0.68
3	0.70	0.675
4	(0.40) 0.69	(0.40) 0.67
5	0.73	0.72
6	0.92	0.91
7	0.57	0.57

I. With Indeni 33kV buses split
II. With Indeni 33kV buses coupled

Operating the 33kV busbar at Indeni in closed state (case II in Table 8) may solve the outage problem for other loads in the plant but does not improve the dip magnitude at the 6kV buses. In fact in some cases the retained voltage even goes lower than case I.
Table 9 shows how the regions of vulnerability are affected if LL(G) or LLLG faults are considered . With LL(G) faults the vulnerability region extends from category 2 to 7. All fault categories pose a risk of voltage sags if LLLG faults are considered though Category 1 and 6 faults still show less severe dips.

Table 9: 6kV Dip magnitude caused by LL(G) and LLLG faults [pu]

Category	LL(G)	LLLG
1	0.90	0.88
2	0.18	0.18
3	0.02	0.03
4	(0.37) 0.65	(0.32) 0.60
5	0.15	0.15
6	0.73	0.73
7	0.01	0.01

From the foregoing the power quality monitors can be located at Indeni on each 33kV incomer and at Skyways on either side of the 66/33kV transformers to counter check each of the two utilities (CEC or Zesco) recordings.

We now come to the assessment of the location methods in the Zambian grid. From the five monitoring locations mentioned earlier four sag source methods were assessed. The first three Reactive Power Method (RP), Distance Relay Method (DR), Slope of System Trajectory Method (SST) are as recommended from section 6.1 The fourth one, Voltage Magnitude comparison is being tried since this portion of the network has only one source. The performance of the methods is indicated in the graphs that follow. However

graphs are presented for only three monitoring positions namely Skyways33, Indeni33A and Indeni33B.

The analysis of results by SST method took a different approach. As seen in section 6.1.2 the SST presents results per phase. The slopes in each of the phases (A, B, C) can have the same or different polarity depending on the fault type and location in the system in relation to Dy transformers which mainly modify dip types. Two evaluation approaches were considered.

1) Based on the faulted phase and applied wholesomely at all monitoring positions irrespective of voltage level and transformer configuration in between the fault point and the monitor position.
2) Using the phase with the lowest dip magnitude as an indicator for the sag source. Unlike the first approach this differentiated between voltage levels as it took the transformer configuration into perspective.

In the first approach LG and LLLG faults are easily analyzed as only one phase is considered. However for LL or LLG faults it becomes difficult as the faulted phases have to give the same slope polarity to indicate direction otherwise with different polarities an indecision is registered.

In the second approach if a fault being considered is at the same voltage level as the monitor position, then for LG faults the faulted phase gives the lowest dip magnitude. This gives the same results as the first evaluation approach. If a LG fault is transformed to a different voltage level through a star-star transformer grounded on both sides, the same faulted phase still gives the lowest dip magnitude on the other voltage level. Referring to Figure 48 with dip propagation in the fault current path, the sag magnitude in pu terms at A is higher than that at C but the sag magnitudes at A, B and D are equal. Propagation of LG faults through a Delta-star transformer will change dip magnitude to the other phases.

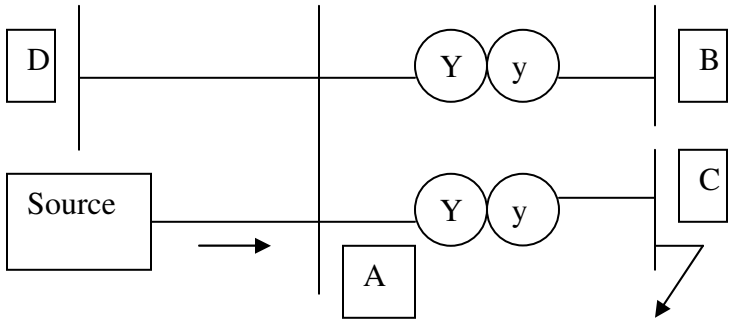

Figure 48: Illustration of dip propagation

Though approach 1) for SST method may have given acceptable results the more rational way is the approach given by 2).

Figure 49 to Figure 52 show how the location methods respond to a LG fault on the 6kV side of the 33/6kV transformer B at Indeni i.e. downstream of Skyways33 and Indeni 33B and upstream of Indeni 33A (see Figure 47).

In Figure 49 we see that at Skyways33 the impedance during the sag reduces and its angle is positive meaning a downstream fault. At Indeni 33A there is no change in the impedance before and during the fault and irrespective of the sign of the angle this indicates an upstream fault. The monitor at Indeni 33B shows that the during-sag

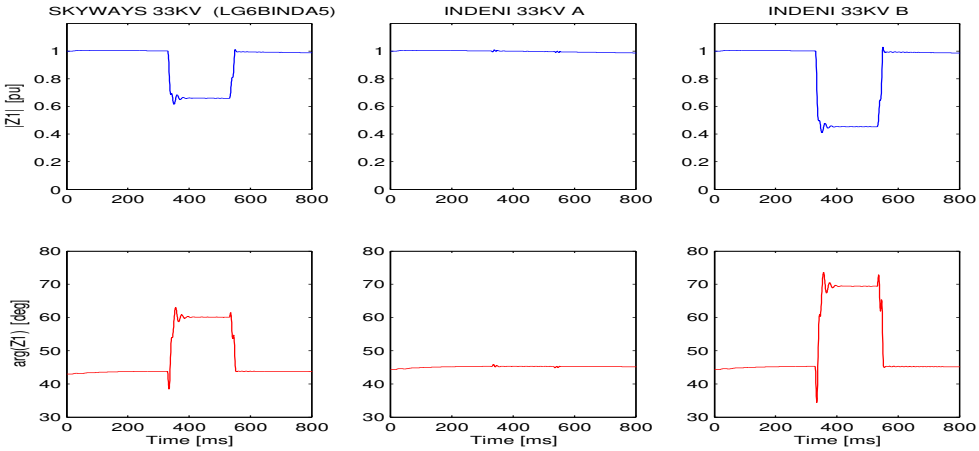

Figure 49: DR Method for LG fault at Indeni 6kV bus B

impedance reduces and its angle is positive also indicating a downstream fault.

Figure 50 shows that at Skyways33 there is a positive deflection in reactive power indicating a downstream fault. At Indeni 33A there is a negative deflection of reactive power indicating an upstream fault. A downstream fault is indicated by the monitor at Indeni 33B as it has a positive deflection of reactive power.

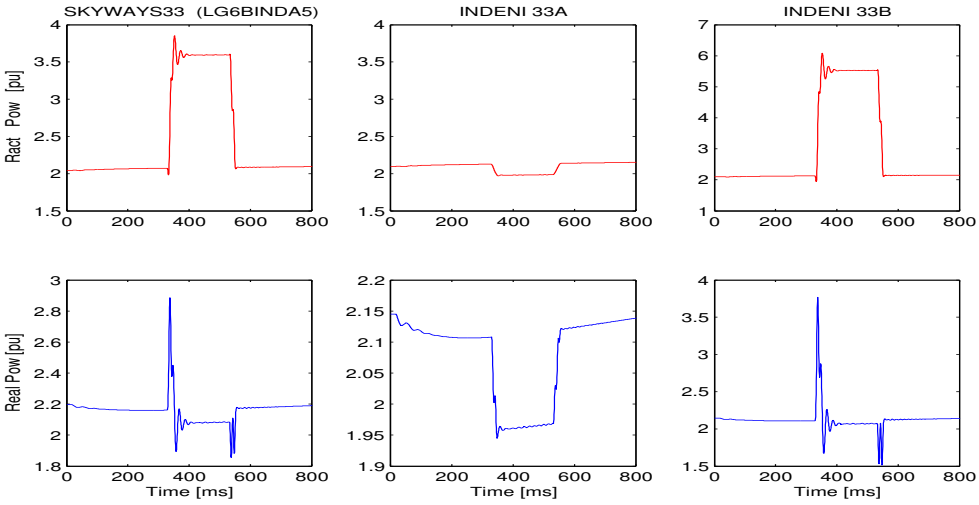

Figure 50: RP Method for LG fault at Indeni 6kV bus B

Figure 51 provides the phase with lowest dip magnitude to use at a corresponding location in Figure 52 to indicate the sag source direction. Coincidentally we see that phase A provides the lowest dip magnitude for the three monitoring positions.

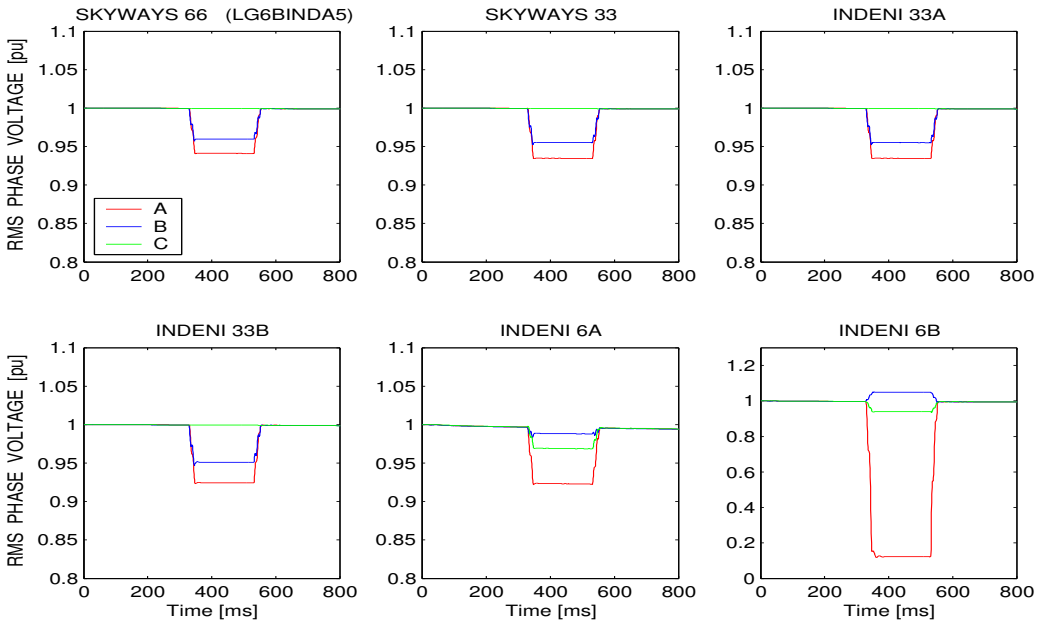

Figure 51: RMS Voltage plot (Dip Magnitude) for LG fault at Indeni 6kV bus B

Figure 52 shows that Skyways33 has a negative slope indicating a downstream fault, Indeni 33A has a positive slope indicating an upstream fault and Indeni 33B has a negative slope indicating a downstream fault.

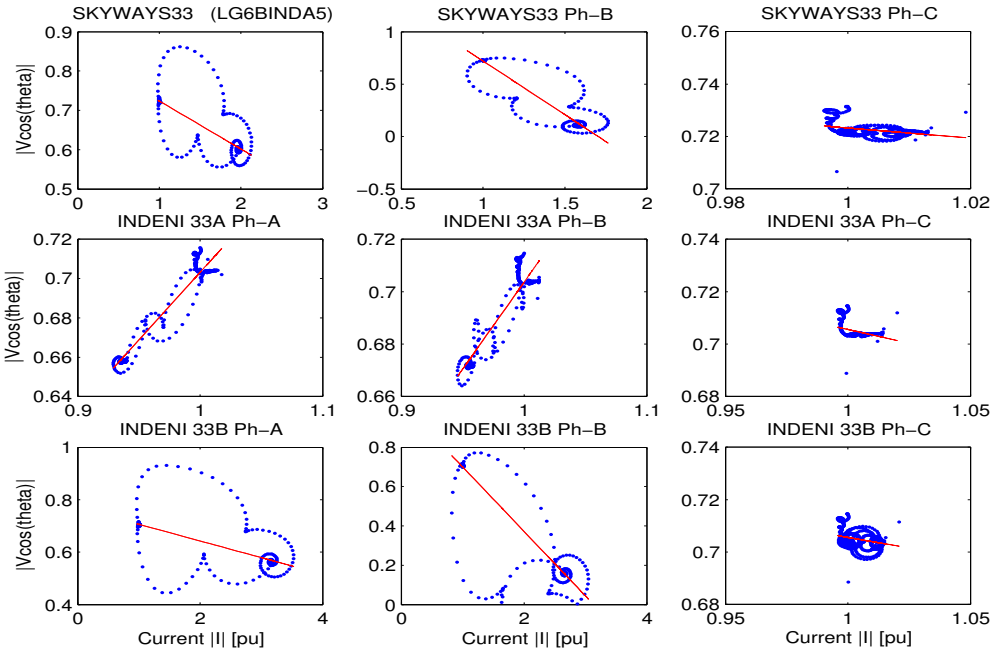

Figure 52: Slope System Trajectory Method for LG fault at Indeni 6kV bus B

Figure 53 to Figure 56 show how the location methods respond to a LG fault on the 400V side of the 6/0.4kV transformer 7 at Indeni.

In Figure 53 the distance relay method indicates downstream fault at both Skyways33 and Indeni 33A as the during-sag impedance reduces and the angle is positive. At Indeni 33B the during-sag impedance remains the same as the pre-sag impedance while its angle is positive. This indicates an upstream fault.

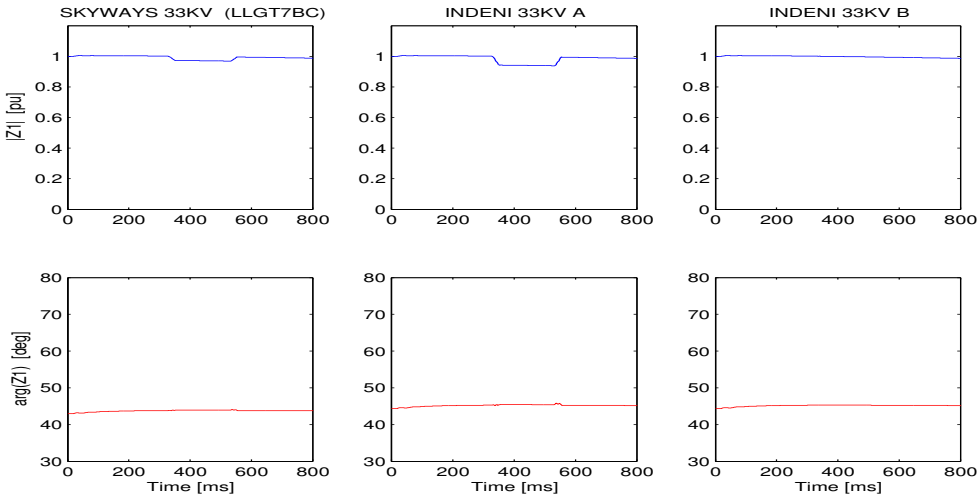

Figure 53: DR method for LGT7BC fault

In Figure 54 the reactive power method shows positive deflections at Skyways and Indeni 33A signifying downstream fault. At Indeni 33B a negative deflection is shown indicating an upstream fault.

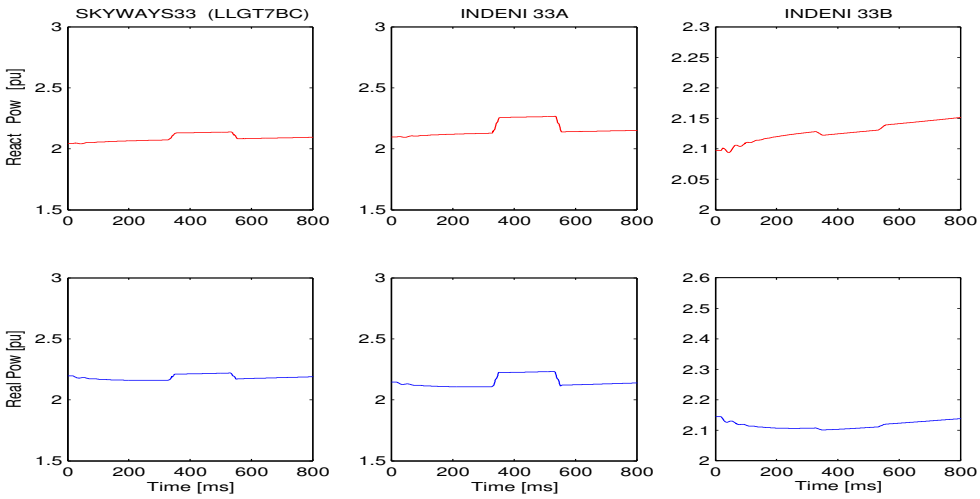

Figure 54: RP method for LGT7BC fault

Figure 55 gives the phase with lowest dip magnitude at a particular location to be used in Figure 56 to indicate sag source direction for the SST method. Incidentally phase A has the lowest dip magnitude at Skyways33, Indeni 33A and Indeni 33B. At Skyways and

Indeni 33A the fault is indicated correctly as downstream as the slope are negative in both cases. At Indeni 33B the slope in phase A is also negative signifying a downstream fault. However this is a wrong indication as the fault is upstream for this bus.

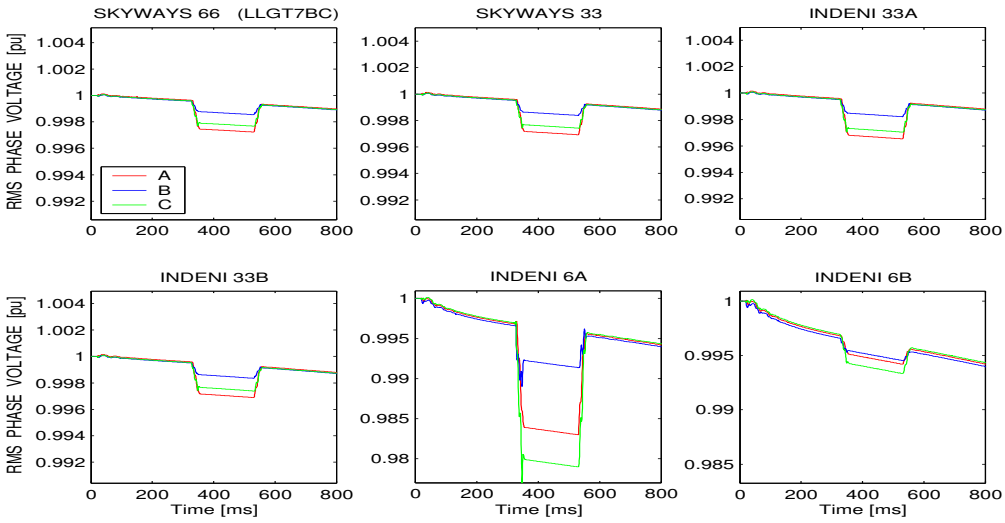

Figure 55: RMS voltages for LGT7BC fault

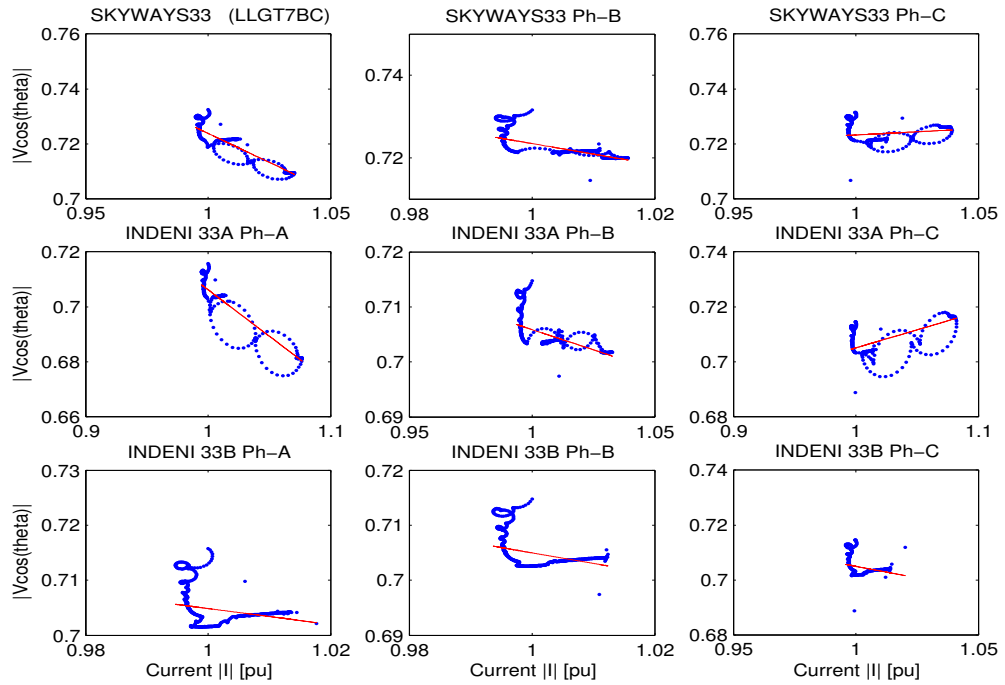

Figure 56: SST method for LGT7BC fault

Figure 57 to Figure 59 show how the location methods respond to a LL fault at Ndola Lime 33kV busbar.

In Figure 57 the distance relay method correctly indicates sag source direction at the three monitoring locations downstream for Skyways33 and upstream for both Indeni 33A and Indeni 33B.

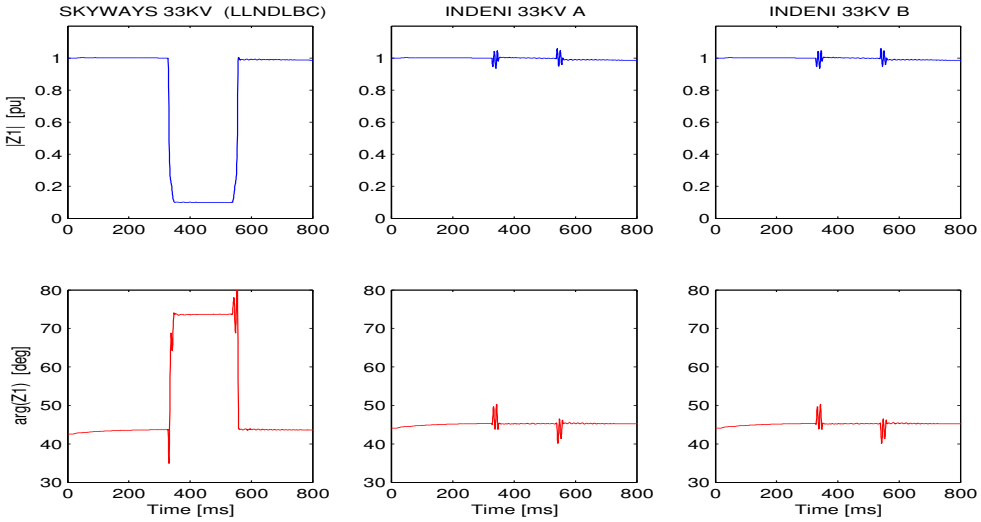

Figure 57: DR method for LLGNDLBC fault

In Figure 58 the reactive power method shows positive deflections at Skyways indicating a downstream fault while at Indeni 33A and Indeni 33B there are negative deflections signifying upstream fault.

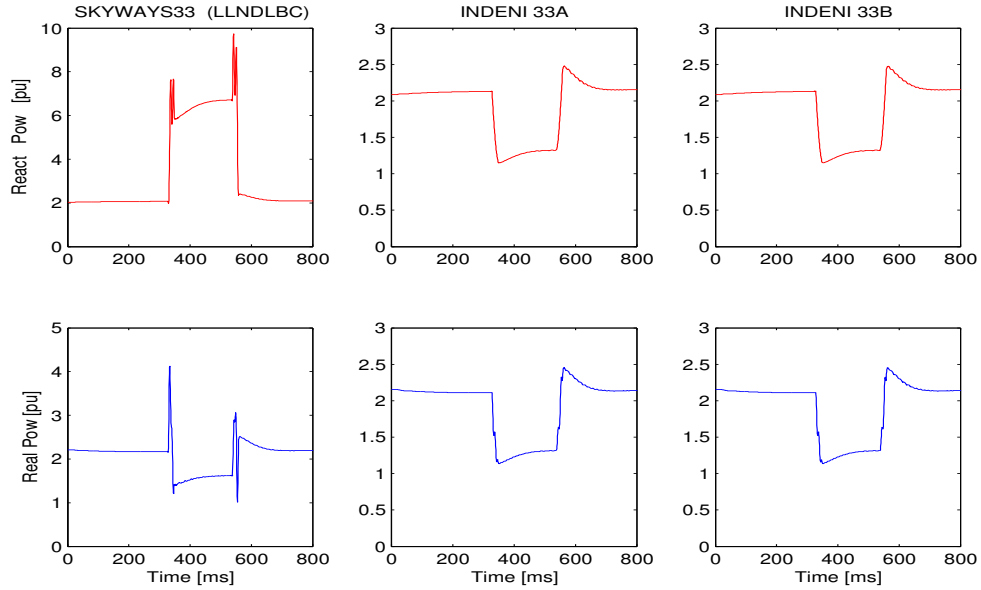

Figure 58: RP method for LLGNDLB fault

AS the fault is at the same voltage level as the monitoring positions we can just use the faulted phases to indicate sag source direction at each location in Figure 59. This is a LL fault in phases B-C. For each of the three monitoring locations phase B and C show same slope sign. Therefore at Skyways 33 the sag source is downstream as the polarities are

negative and at Indeni 33A and Indeni 33B the polarities are positive indicating upstream fault.

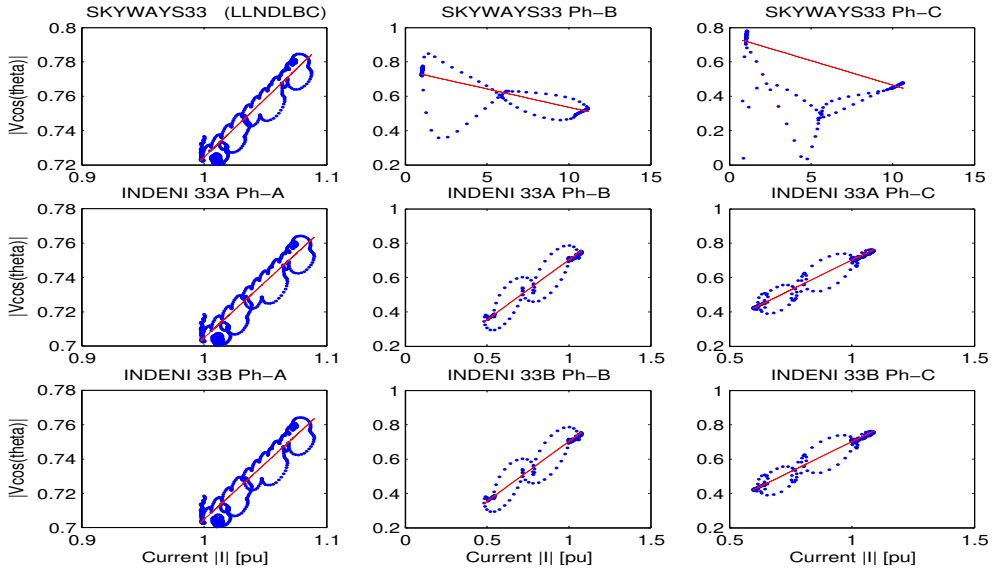

Figure 59: SST method for LLGNDLBC fault

The overall performance of the location methods for all of the above seven fault categories is summarized in the Table 10 below.

Table 10 : Performance of location methods

Monitor Location	Reactive Power (RP) [%]	Distance Relay (DR) [%]	Slope of System Trajectory (SST)	
			Faulted Phase [%]	Dip Mag [%]
Maposa 66	100	100	91	100
Skyways 66	97	100	85	100
Skyways 33	94	100	85	100
Indeni 33A	100	100	85	91
Indeni 33B	100	100	85	91

Table 10 shows that the distance relay method gives good performance for all the monitoring positions in all the 68 fault scenarios considered. The results of the reactive power method were such that out of the 68 fault simulations, only five resulted in wrong sag source direction indication. This was actually for a monitor at the faulted bus (Skyways 33kV). The slope of system trajectory methods (using dip magnitude to indicate direction) shows lower performance at Indeni 33A and Indeni 33B. This is mainly caused by faults from the 400V system. It was observed that for all faults on the 400V system one of the monitors at Indeni 33kV busbar (Indeni 33A or Indeni 33B) which is not in the fault path would always give wrong sag source direction.

The dip magnitudes at the locations shown in Figure 51 for a LG fault at Indeni 6kV bus B can be summarized as in Table 11

Table 11: Voltage magnitude comparison for a LG fault at Indeni 6B

Monitor Location	Dip Magnitude [pu]	
	HV	LV
Skyways 66/33kV	0.942	0.935
Indeni 33/6kV A	0.935	0.924
Indeni 33/6kV B	0.925	0.120

Comparing the voltage magnitudes on either side of each transformer we see that at all three locations the LV side of the transformers have the lowest sag magnitude indicating that the sag source is on the LV side. But Indeni 6kV buses are not connected together and we don't have simultaneous faults. Additionally sag magnitude at Skyways 33 and Indeni 33A have the same value signifying propagation at the same voltage level. However sag magnitude at Indeni 33B is lower than the former two. This is due to the voltage drop caused by the fault current flow. So comparing the sag magnitudes on Indeni 6kV buses we conclude that the fault was on Indeni 6kV bus B.

The Voltage Magnitude Comparison Method is easy if dip propagation at the same voltage level or in a network with only star–star transformers which are grounded on both sides is considered. Star-star transformers grounded on both sides do not affect voltage propagation i.e the zero sequence component is not blocked. The method becomes difficult to apply when delta-star transformers and distributed generation (DG) are involved as dip type changes and the DG keeps up voltages at nearby buses.

6 MEASUREMENTS

The circuit used for measurements is a scaled model of a 400kV transmission line. The model has six π-sections each of which represents a distance of 150km on the actual transmission line. The model is operated at 400V and its line parameters are:

$L_m = 2.05mH$ $R_m = 0.05\Omega$ $C_m = 46\mu F$

In the measurement set ups the capacitance C_m was not used.

Figure 60 below shows the circuit arrangement for radial measurements. The loads at both bus A and C were 9kW three-phase resistive loads operating at almost unity power factor. LG, LL, LLG and LLLG faults were simulated at A and B for upstream and C for downstream of the PQ monitor.

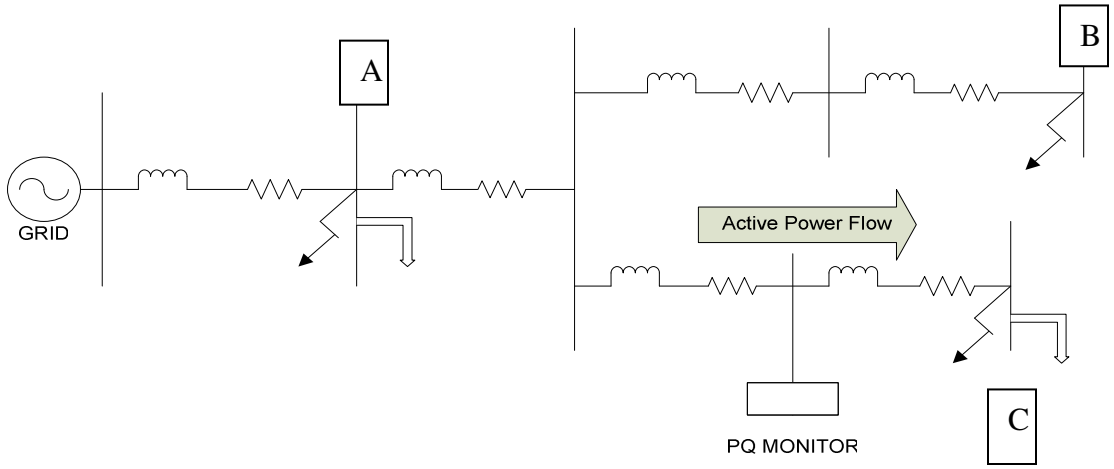

Figure 60: Laboratory set up for radial measurements

Figure 61 show the circuit arrangement for co-generation measurements. The 9kW loads as in the radial set up were used and still operating at almost unity power factor. As before LG, LL, LLG and LLLG faults were simulated at A and B.

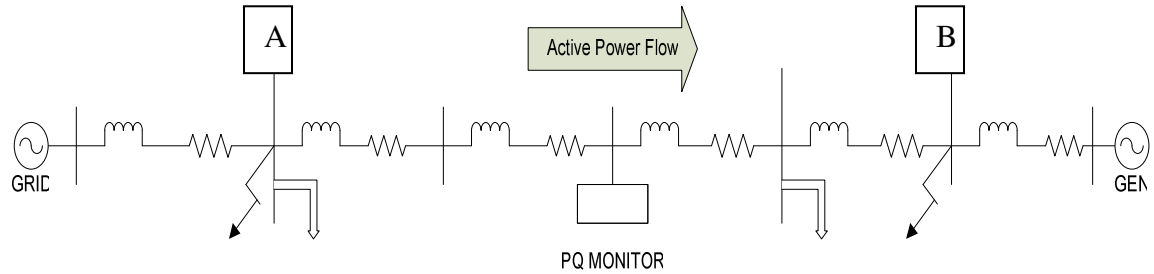

Figure 61: Laboratory set up for co-generation measurements

In general for both radial and co-generation set ups the faulted phase for LG faults was A and for LL and LLG faults was B-C. The fault resistance was zero and the fault duration was about 60ms. The power quality monitoring equipment used is the Dranetz Power Platform (PP1).Measured data was channeled through Dran-view and exported to MATLAB for post processing.

The results are indicated in Figure 62 to Figure 73 below. The plot indicates the fault type and the information contained in the top left subplot in brackets is the system configuration and sag direction i.e.

- Radial DS for radial system and downstream fault
- Radial US for radial system and upstream fault
- Co-gen DS for co-generation system and downstream fault
- Co-gen US for co-generation system and upstream fault

Figure 62 below shows how the distance relay method responds to downstream LLLG, LLG, and LG faults close to the monitoring position in a radial system. In all three cases the positive sequence impedance during the disturbance reduces and the angles are positive indicating downstream faults.

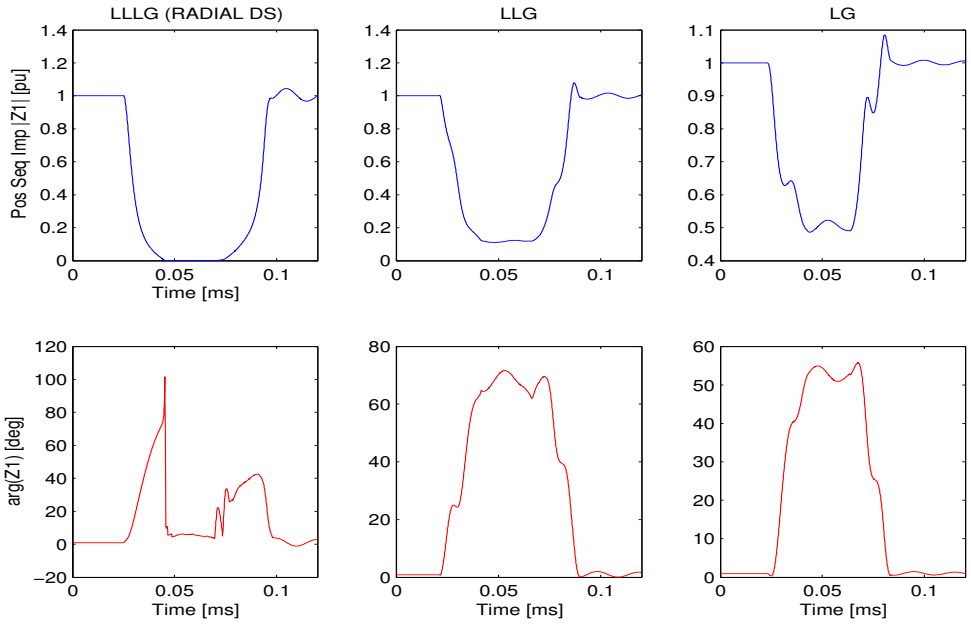

Figure 62: DR Method for radial downstream system faults

Figure 63 shows how the reactive power method responds to the same faults shown in Figure 62. The reactive power method shows some positive deflections but these can be considered as transitions from one steady state to another. At this stage we can say the reactive power method is indecisive partly because there was little reactive in the system as the load operated at almost unity power factor.

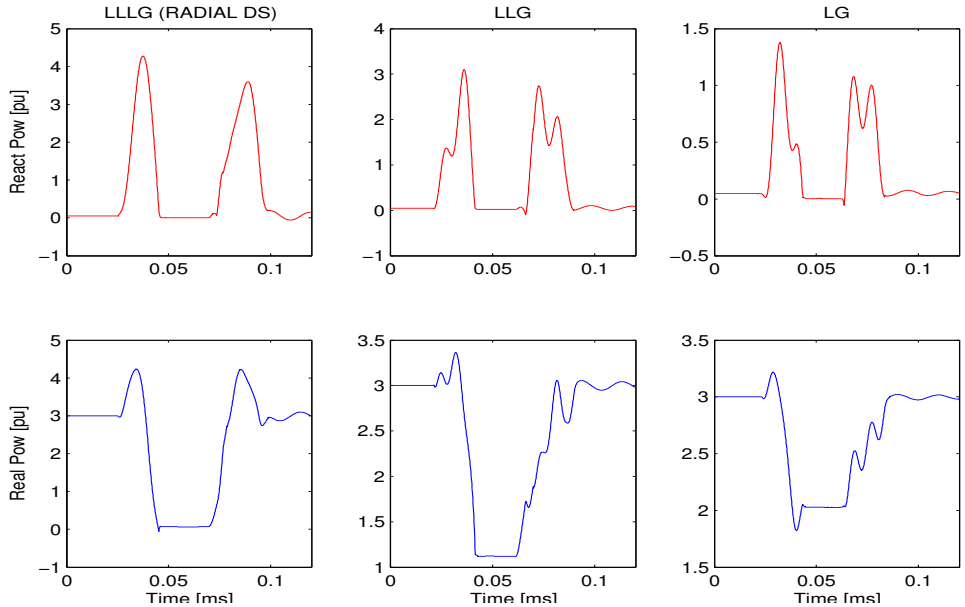

Figure 63: RP Method for radial downstream system faults

Figure 64 shows how the slope of system trajectory method applied to the same faults of Figure 62 and Figure 63. As this is a radial system with no transformers (D-y) involved the faulted phase(s) is used for sag source direction indication. This gives downstream sag source for the three fault types.

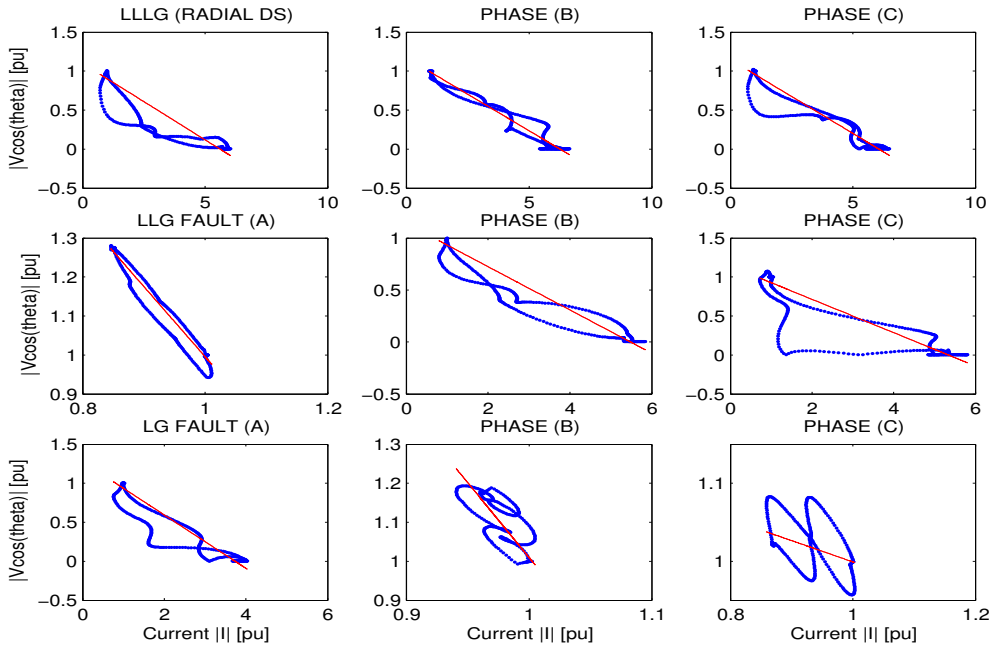

Figure 64: SST Method for radial downstream system faults

Figure 65 to Figure 67 show the three location methods for upstream faults in radial system configuration.

In Figure 65 positive sequence impedance can be considered as not varying between pre-fault and during-fault. This therefore indicates upstream fault for the three fault types.

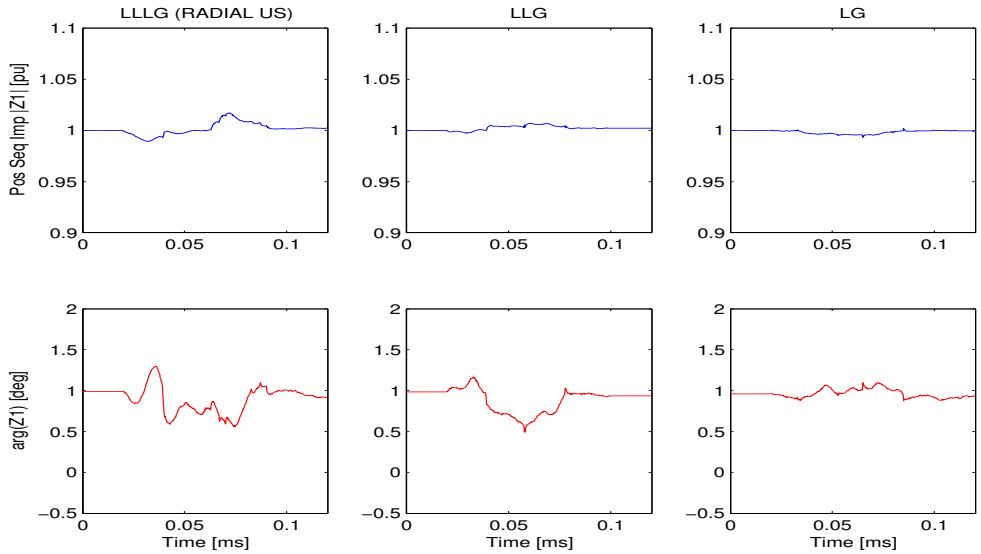

Figure 65: DR Method for radial upstream system faults

In Figure 66 whilst operating with positive pre-fault reactive power there is a negative deflection during the disturbance for all three fault types. This is an indication of upstream fault in each fault type.

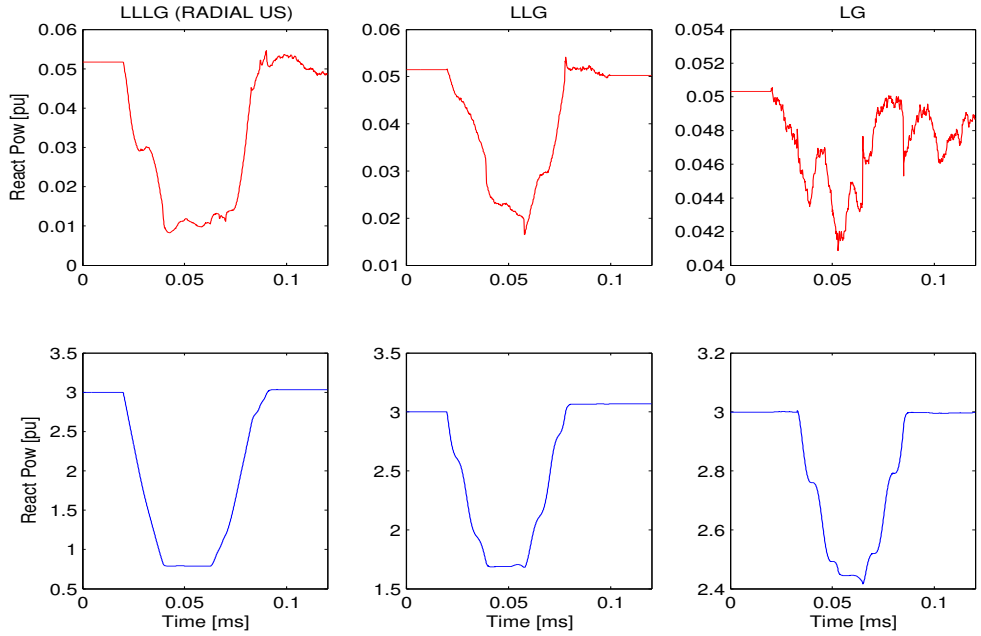

Figure 66: RP Method for radial upstream system faults

Figure 67 shows that for the LG fault phase A has positive slope indicating an upstream fault. The LLG case shows phases B and C having positive slopes also indicating an upstream fault. The LLLG fault shows positive slopes in all the three phases and this also indicates an upstream fault.

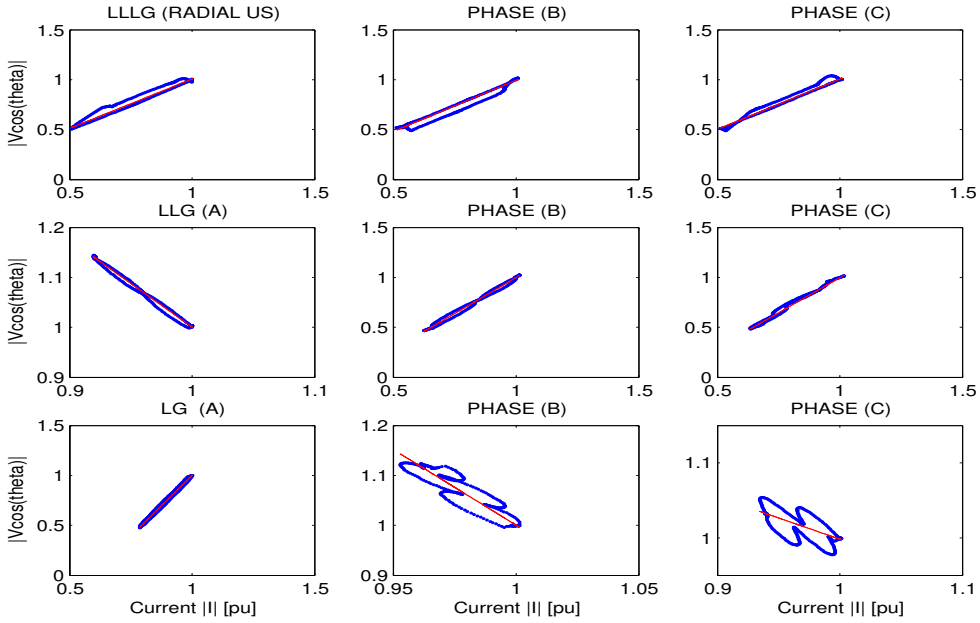

Figure 67: SST Method for radial upstream system faults

Figure 68 through to Figure 73 indicate results of measurements in the co-generation set up. Figure 68 shows that in the distance relay method the positive sequence impedance reduces in value during the disturbance and the angles are positive for the three fault types. This signifies downstream fault.

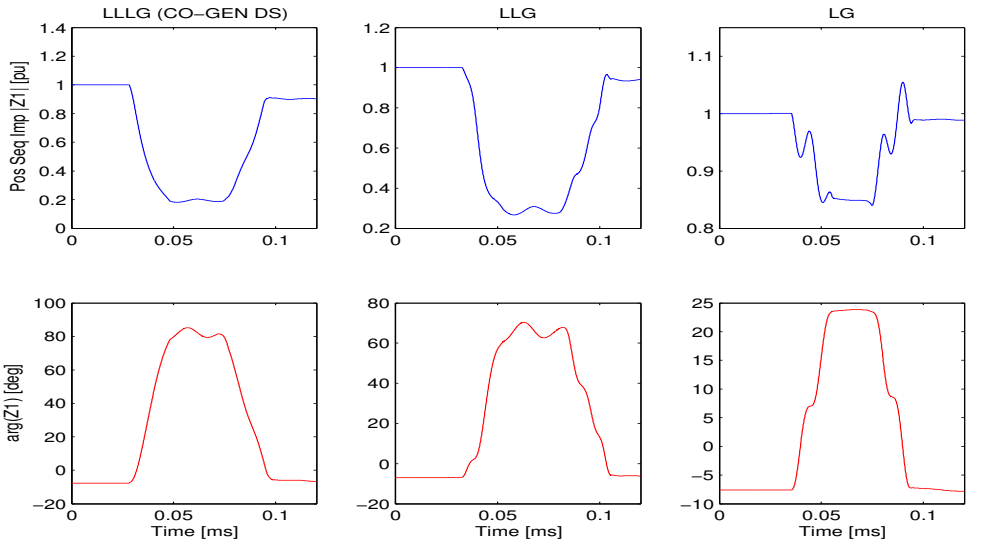

Figure 68: DR Method for Co-generation downstream system faults

Figure 69 show how for downstream faults the reactive power changes sign from a negative pre-fault value to a positive value during the fault. All the three fault type show this behavior. This confirms the proposal arrived at with PSCAD/EMTDC simulations in the Brazilian and Zambian networks.

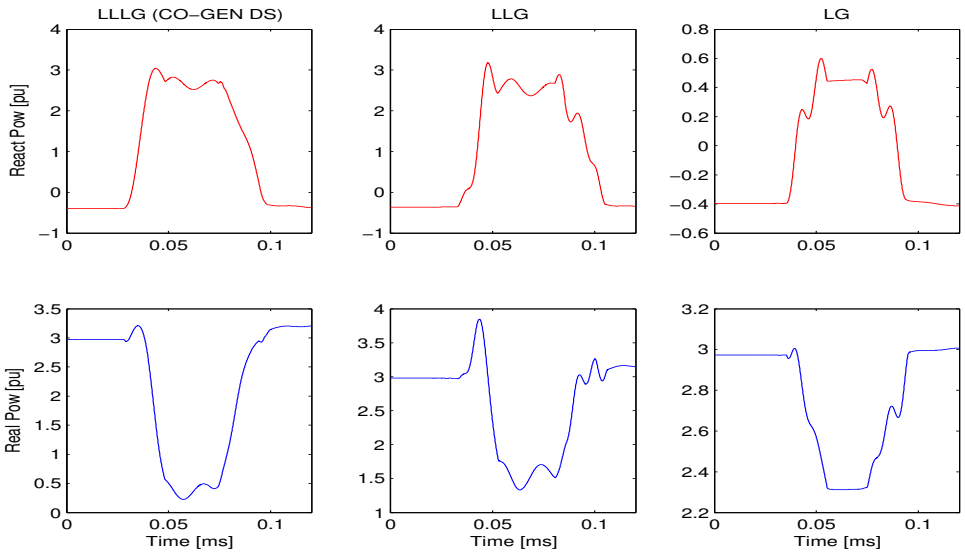

Figure 69: RP Method for Co-generation downstream system faults

Figure 70 shows that for the LG fault phase A has negative slope indicating a downstream fault. The LLG case shows phases B and C having negative slopes also indicating downstream fault. The LLLG fault shows negative slopes in all the three phases again indicating downstream fault.

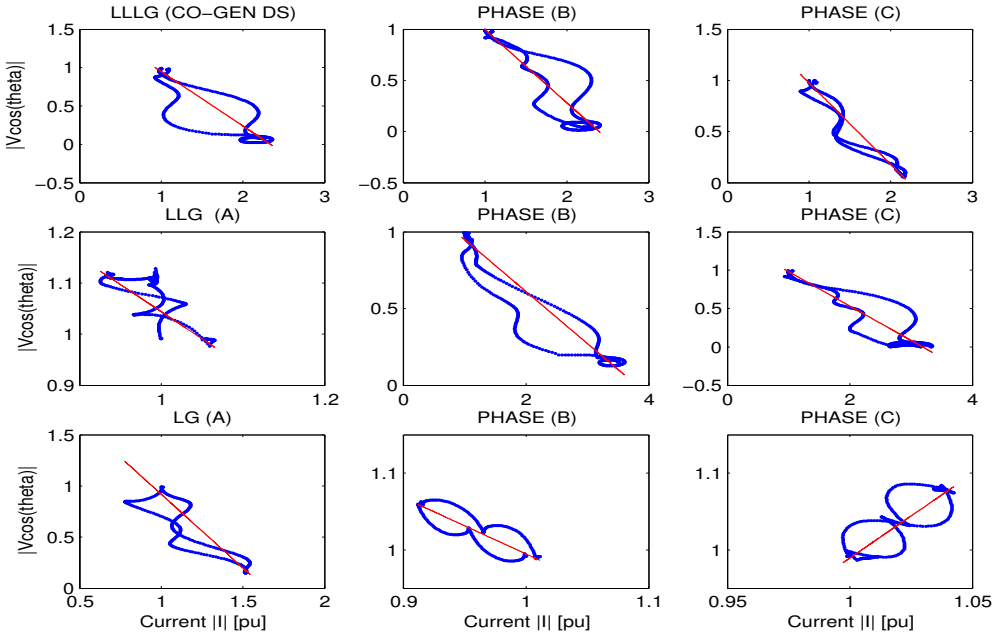

Figure 70: SST Method for Co-generation downstream system faults

Figure 71 shows that in the distance relay method the positive sequence impedance reduces in value during the disturbance and the angles are negative for the three fault types. This signifies upstream sag source for each fault type.

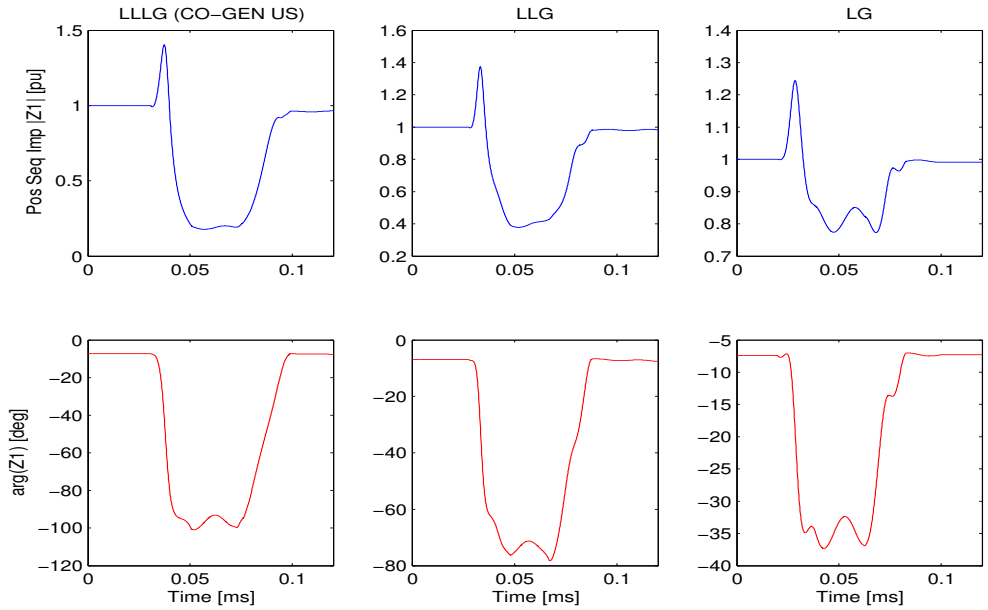

Figure 71: DR Method for Co-generation upstream system faults

Figure 72 shows a negative deflection for a point operating with negative reactive power. This is considered as upstream sag source and is correctly indicated for each fault type.

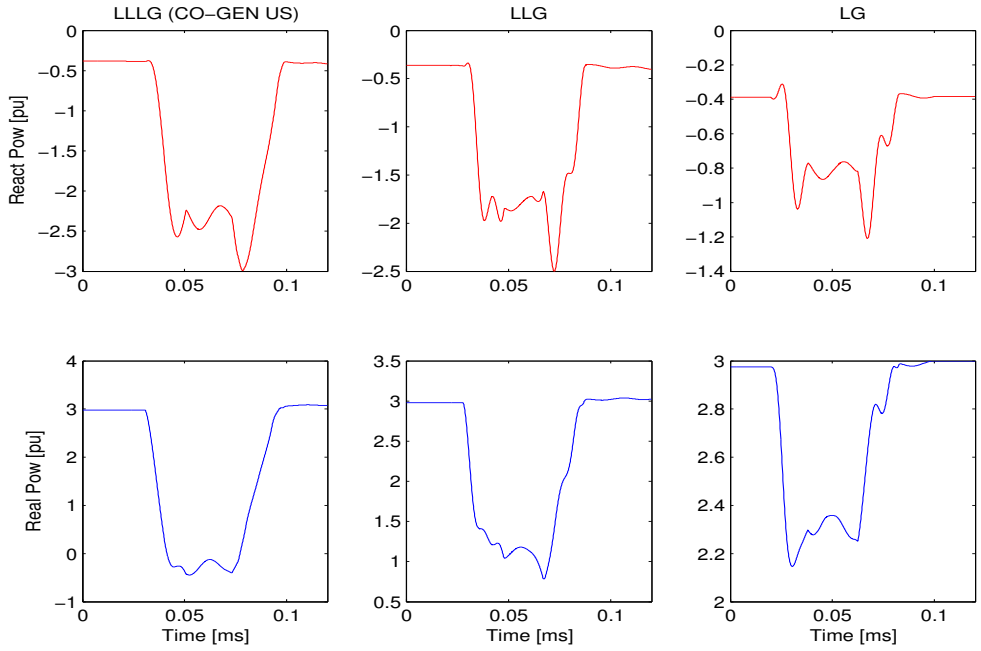

Figure 72: RP Method for Co-generation upstream system faults

Figure 73 shows that for the LG fault phase A has negative slope indicating a downstream fault. The LLG case shows phases B and C having negative slopes also indicating downstream fault. The LLLG fault shows negative slopes in all the three phases again indicating downstream fault. However the sag source direction is indicated wrongly for each fault. This is because there is reversal of active power flow as indicated in the bottom part of Figure 72 for the LLLG fault (active power goes negative). The LLG and LG do not show active power reversal though. Perhaps if the power is considered per phase this could show. Hence if active power reversal is taken into account the sag source for the SST method in Figure 73 can be said to be upstream.

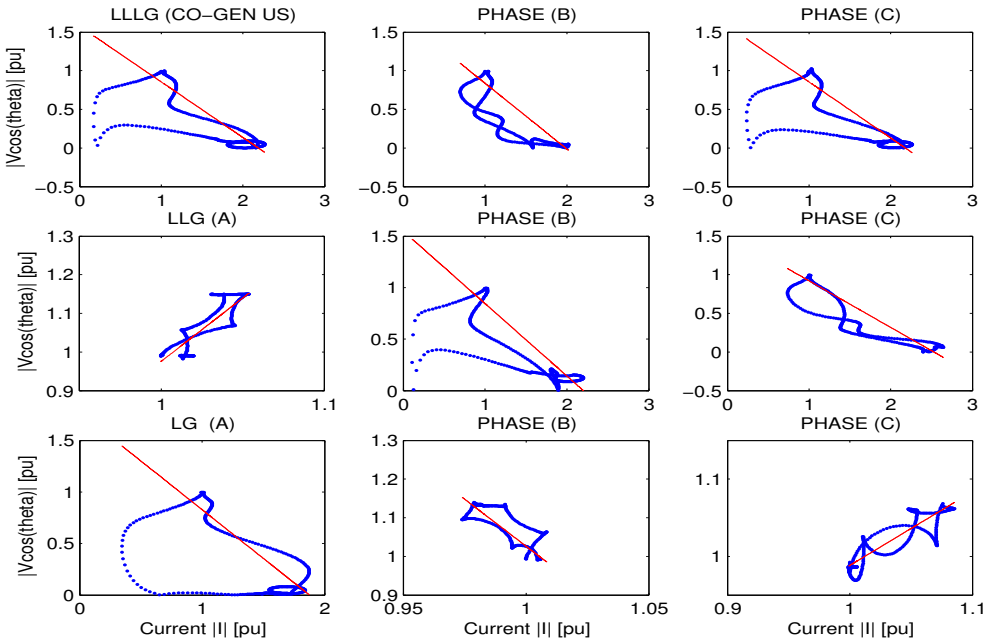

Figure 73: SST Method for Co-generation upstream system faults

Table 12 below presents a summary of the results obtained with laboratory measurements. It even includes results for LL faults which were not shown in the preceding graphs. Note that the results for the SST method in the co-generation upstream faults are corrected to read as upstream because of active power reversal.

The distance relay method and the slope of system trajectory method show good results. In radial systems the distance relay method may sometimes give oscillatory positive sequence impedance plots making it difficult to indicate sag source direction. When using the slope of system trajectory method in co-generation systems care should be taken to note any incidence of reversal of active power flow as has been noted in the Brazilian network and laboratory measurements. Both distance relay and reactive power methods perform well in the co-generation configuration. The reactive power method is however affected by close up faults as seen in Figure 63 above.

Table 12: Laboratory Measurements

System	Fault Position	Fault Type	Location Method		
			DR	RP	SST
Radial	Downstream	LG	Downstream	Indecisive	Downstream
		LL	Downstream	Indecisive	Downstream
		LLG	Downstream	Indecisive	Downstream
		LLLG	Downstream	Indecisive	Downstream
	Upstream	LG	Upstream	Upstream	Upstream
		LL	Upstream	Upstream	Upstream
		LLG	Upstream	Upstream	Upstream
		LLLG	Upstream	Upstream	Upstream
Co-Gen	Downstream	LG	Downstream	Downstream	Downstream
		LL	Downstream	Downstream	Downstream
		LLG	Downstream	Downstream	Downstream
		LLLG	Downstream	Downstream	Downstream
	Upstream	LG	Upstream	Upstream	Upstream
		LL	Upstream	Upstream	Upstream
		LLG	Upstream	Upstream	Upstream
		LLLG	Upstream	Upstream	Upstream

7 CONCLUSIONS

In PSCAD/EMTDC simulations the performance of the distance relay method was such that it gave correct sag source indication all the time. As regards measurements in the lab it was excellent when applied to the co-generation system. The results obtained for upstream faults in the radial system configuration though giving correct sag source indication were not very convincing.

The reactive power method like the distance relay method was also excellent in the co-generation system. Though the system set up in the laboratory measurements had very little reactive power flow the method was still able to distinguish correctly between upstream and downstream faults in the radial system except for the close-up fault case..

The sign of the pre-fault operating value of reactive power is crucial in determining the sag source direction. From a negative operating value to any value within the negative zone including zero reactive power the sag source is considered upstream. A downstream sag source results if the reactive power changes from a negative value in pre-fault to a positive value during the fault. However for a point operating with positive pre-fault reactive power only the deflection polarity is necessary to indicate sag source: positive for a downstream fault and negative for an upstream fault. The reactive power method is affected by close up faults i.e. the method may give wrong sag source indication for faults at the monitoring bus.

The slope of system trajectory method is easy to apply in purely radial systems and where the transformers are star-star and grounded on both sides. Balanced faults give good results. The method can also be applied to systems with D-y transformers. However in this case an extra decision parameter is required when identifying sag sources due to unbalanced faults. This parameter identifies which phase(s) to use to give sag source indication at a particular monitoring point. The phase with lowest dip magnitude is used as the phase to give sag source direction.

When applied to co-generation networks besides the requirement to know the lowest dip magnitude at a point there is need to check for current (active power) reversal. If active power reversal is detected the fault is upstream.

The real current component method though not applied further to the Zambian grid and laboratory measurements has comparable performance to the slope of system trajectory method. Though the original form of this method in [12] used the polarity of initial deflection this thesis considered the polarity in the during-fault steady state as processing was done with FFT which does not perform well with non-stationary signals.

The Zambian case study focused on two issues. To determine the vulnerability of the sensitive load at Indeni 6kV buses to both internal and external faults of the plant. Secondly to further prove the location methods initially tested with the Brazilian network.

Results were that internal faults on the 400V system do not affect the sensitive loads at Indeni 6kV buses even when three phase faults are considered. Faults within the Indeni 6kV system resulted in less severe dips for sensitive load buses. The lowest obtained from a three phase fault was 0.88 pu.

The sensitive loads at Indeni are vulnerable to sags caused by faults from both the CEC and Zesco networks. From the CEC network categories contributing to this are the 66kV supply line into Ndola and the 66kV and 220kV network upward of Maposa Substation. Faults on the 66kV CEC Luanshya system do not contribute to sags for sensitive loads at Indeni for LG faults but have an effect when LL(G) and LLL(G) faults are considered. From the Zesco network the contribution is from the 33kV lines out of Skyways Substation as well as faults on the 11kV system at Skyways Substation.

The performance of the location methods in the Zambian grid was that the distance relay method was 100% on target at each of the five monitoring points. The reactive power method was on average 98.2% correct and the average performance for the slope of system trajectory method was 96.4%. Again the reactive power method showed that it is affected by close up faults.

Future work would involve installing monitors at the three selected locations Skyways 33, Indeni 33A and Indeni 33B in the Zambian network. Field data will then be obtained for analysis with the three location methods distance relay, reactive and slope of system trajectory.

8 BIBLIOGRAPHY

[1] IEEE 1159-1995 Recommended Practice for Monitoring Electric Power Quality.

[2] Math H. J. Bollen, “Understanding Power Quality problems: Voltage Sags and Interruptions”, IEEE Press, 2000

[3] IEC 61000-4-30

[4] Math H. J. Bollen, Irene Y. H. Gu, “Signal Processing of Power Quality Disturbances”, IEEE Press, July 2006

[5] Rafael Flores, Signal Processing Tools For Power Quality Event Classification, Licentiate, Chalmers University of Technology, Göteborg, Sweden, 2003

[6] Ashok Kumar Pradhan, Aurobinda Routray, Applying Distance Relay for Voltage Sag-Source Detection, IEEE Trans. Power Del.

[7] J. Gomez, M. Morcos, D Tourn, M. Felici, A Novel Methodology to locate originating points of voltage sags in Electric Power Systems, CIRED Intl. Conf. Elec. Dist.

[8] C. Li, T. Tayjasanannt, W. Xu, X. Li, Method for voltage-sag-source detection by investigating slope of the system trajectory, IEE Proc. Gen. Trans. Distribution

[9] Thavatchai Tayjasanant, Chun Li, Wilsun Xu, A resistance Sign-Based Method for Voltage Sag Detection, IEEE Trans. Power Del

[10] A.C. Parsons, W.M. Grady, E.J. Powers, J.C. Soward, A Direction Finder for Power Quality Disturbances Based Upon Disturbance Power and Energy, IEEE Trans. Power Delivery

[11] Sean-Ju Ahn, Dong-Jun Won, II-Yop Chung & Seung-II Moon, Determination of the Relative Location of Voltage Sag Source According to Event Cause, IEEE

[12] N Hamzah, A Mohamed, A Hussain, A new Approach to Locate the Voltage Sag Source Using Real Current Component, ELSERVIER

[13] D.G Hart, W. Peterson, David Uy, J Schneider, D. Novosel, R Wright, Tapping Protective Relays for Power Quality Information, IEEE

[14] Roberto C. Leborgne, Daniel Karlsson, Jaap Daalder, Voltage Sag Source Location Methods Performance Under Symmetrical and Asymmetrical Fault Conditions, IEEE